

Star Formation in Dwarf Galaxies of the Nearby Centaurus A Group

Stéphanie Côté and Adam Draginda¹

*Canadian Gemini Office, HIA/NRC of Canada, 5071 West Saanich Rd., Victoria, B.C., Canada,
V9E 2E7*

Stephanie.Cote@nrc-cnrc.gc.ca

Evan D. Skillman

Astronomy Department, University of Minnesota, Minneapolis, MN 55455

skillman@astro.umn.edu

and

Bryan W. Miller

AURA/Gemini Observatory, Casilla 603, La Serena, Chile;

bmillier@gemini.edu

ABSTRACT

We present $H\alpha$ narrow-band imaging of 17 dwarf irregular galaxies (dIs) in the nearby Centaurus A Group. Although all large galaxies of the group are or have been recently through a period of enhanced star formation, the dIs have normal star formation rates and do not contain a larger fraction of dwarf starbursts than other nearby groups such as the Sculptor Group or the Local Group. Most of the galaxies in the group now have fairly accurately known distances, which enables us to obtain relative distances between dIs and larger galaxies of the group. We find that the dI star formation rates do not depend on local environment, and in particular they do not show any correlation with the distance of the dI to the nearest large galaxy of the group. There is a clear morphology-density relation in the Centaurus A Group, similarly to the Sculptor Group and Local Group, in the sense that dEs/dSphs tend to be at small distances from the more massive galaxies of the group, while dIs are on average at larger distances. We find four transition dwarfs in the Group, dwarfs that show characteristics of both dE/dSphs and dIs, and which contain cold gas but no current star formation. Interestingly the transition dwarfs have an average distance to the more

¹Present address: Canada-France-Hawaii Telescope Corporation, 65-1238 Mamalahoa Highway, Kamuela, HI 96743; draginda@cfht.hawaii.edu

massive galaxies which is intermediate between those of the dEs/dSphs and dIs, and which is quite large: 0.54 ± 0.31 Mpc. This large distance poses some difficulty for the most popular scenarios proposed for transforming a dI into a dE/dSph (ram-pressure with tidal stripping or galaxy harassment). If the observed transition dwarfs are indeed missing links between dIs and dE/dSphs, their relative isolation makes it less likely to have been produced by these mechanisms. An inhomogeneous IGM containing higher density clumps would be able to ram-pressure stripped the dIs at larger distances from the more massive galaxies of the group.

Subject headings: galaxies: dwarf — galaxies: irregular — galaxies: evolution — — HII regions

1. Introduction

The Centaurus A Group of galaxies is one of the closest groups of galaxies outside the Local Group (at a mean distance of about 3.8 Mpc). Its composition is, however, much different from that of the Local Group, being a heterogeneous assembly of early to late-type galaxies, and, in fact, it has the largest dispersion of morphological types amongst all of the 55 nearest groups reported by (de Vaucouleurs 1979). Interestingly, it seems that all of its main galaxy members have been through, or are experiencing, a period of enhanced star formation. The most prominent member of the group is Centaurus A itself (NGC 5128), a giant peculiar elliptical radio galaxy with powerful X-ray and radio jets, which most probably suffered a recent major merger. Both M83 and NGC 5253 are starburst galaxies (Calzetti et al. 1999); NGC 4945 has a Seyfert nucleus (Done et al. 1996) and NGC 5102 is in a post-starburst phase (Davidge 2008). One is then led to wonder if the group’s dwarf galaxy members also share this elevated level of activity. About 50 dwarfs are now known in the group (Karachentsev et al. 2007), of which about two-thirds are gas-rich dwarfs (dIs), and it would be interesting to know if these dIs also have an elevated level of current star formation and a larger fraction of dwarf starbursts than the dwarf galaxy population of less “active” groups, such as the nearby Sculptor Group (Skillman et al. 2003a). In other words, is the star formation activity of the dwarfs influenced by their global group environment, or, does it only depend on local conditions and internal processes?

A reasonable estimate of star formation rates (SFRs) in dwarf galaxies can be obtained by $H\alpha$ imaging, as it is known that in dwarf galaxies infrared and radio emission both can seriously underestimate the star formation rate (e.g., Bell 2003). In the case of the Centaurus A Group dwarfs, most of the dwarfs have relatively accurate distances (e.g., Karachentsev et al. 2002, with distances determined via the tip of the red giant branch method with errors typically of ~ 0.5 Mpc), and with optical diameters ranging from 1 to 10 arcmins they can have their full area imaged easily in one pointing. An $H\alpha$ imaging survey can then produce much better star formation estimates, especially compared to many galaxy studies at higher redshifts for which SFR estimates are derived

from longslit data, for example (Balogh et al. 1997), or even worse from limited aperture fibers such as SDSS or 2dF surveys. As is obvious from Figure 1 below, in some cases most of the star formation activity is found in the outside regions, and a slit passing through the nucleus would severely underestimate the true star formation rate. A detailed survey of HII regions in each dwarf is also useful in order to find individual high surface brightness HII regions required for follow-up spectroscopy for accurate abundance analysis (e.g., Skillman et al. 2003a,b). The vast majority of nearby dwarfs have only been observed through longslits, not multi-object spectroscopy, so it is even more important to know exactly how to position the slit to align them on the brightest HII regions, from which one can reap the largest numbers of fainter emission lines.

Another useful outcome of a $H\alpha$ survey of the dIs members of a group is that one can identify so-called transition dwarf galaxies, dwarfs that show characteristics in their morphology of both early-type dwarfs, dwarf ellipticals (dEs) or dwarf spheroidals (dSphs), and late-type dwarfs (dIs). These transition dwarfs have cold gas but no (or extremely low) active star formation so they will be mostly non-detections in the $H\alpha$ survey. These dwarfs have been proposed as a “missing link” between the two classes of dwarfs (e.g., Grebel et al. 2003). The question as to whether they represent a real evolutionary link between dEs/dSphs and dIs is still controversial. In the Local Group there is a clear morphology-density relation amongst the dwarfs, with dSphs being found predominantly at short distances from large galaxies, while dIs are more spread out in the group. Several scenarios have been proposed to efficiently transform a dI into a dSph in the vicinity of larger galaxies. Did dSphs end up as they are because of internal properties (from genetics), or are they dIs or pre-dIs that transformed into dSphs simply because they happen to be at the wrong place at the wrong time? The study of transition dwarfs in groups might bring clues to their nature, and, indirectly, to the nature of dSphs too.

In §2 we will describe the $H\alpha$ observations, and §3 the SFRs for the Centaurus A Group dwarfs will be derived. Section 4 will present the star formation trends for dIs, its dependence on environment, and will discuss the transition dwarfs in the Centaurus A Group and other groups.

2. Observations

2.1. Target Selection

We observed all of the 19 dwarf irregular (dIs) galaxies members of the Centaurus A Group listed in Côté et al. (1997). Of these, 17 were detected, and are listed in Table 1. CEN5, which was also listed in Côté et al. (1997) as a member dI, was also observed but not detected, and it has recently been confirmed to be instead a background galaxy (Bouchard et al. 2004). It is important for determining membership in nearby groups such as Centaurus A to confirm the HI detections of candidates dIs with an optical radial velocity, or obtain a rough distance estimate through a color-magnitude-diagram (CMD) of the resolved stellar populations. This is necessary because of the possible confusion with Galactic High-Velocity-Clouds (HVCs) which can have HI velocities of

several hundreds of km s^{-1} (as was the case for CEN5). Prior to our observations, all of the dwarfs listed in Table 1 had been confirmed to be bona fide members with optical spectroscopy, except UKS 1424-460 and UGCA 365 for which the memberships were confirmed by tip of the red giant branch distances from HST by Karachentsev et al. (2002, 2007).

Since then, the total number of known dIs in Centaurus A has grown to 28 confirmed dIs and 4 more possible ones. Jerjen et al. (1998) found AM1318-444, not detected in HI but confirmed by optical spectroscopy. Banks et al. (1999), as part of HIPASS, conducted a blind HI survey of the group and proposed 10 new candidate dIs. The more recent HIDEEP survey (Minchin et al. 2003) has revealed an additional possible dI member, J1337-33, and Huchtmeier et al. (2000) shows an HI detection for one more possible dI member, KK170. Although none of these last 12 HI detected dIs has been confirmed with optical spectroscopy, ESO 321-G14, ESO 381-G18, IC 4247, AM1321-304 and HIPASS J1337-39, as well as HIPASS J1321-31, HIDEEP J1337-33 and ESO 269-G58 were all followed-up with HST observations and all had their distances confirmed from their red giant branch tip (Karachentsev et al. 2002, 2007; Grossi et al. 2007). Of these, only the first five appear to be currently forming stars and to probably harbour HII regions, but unfortunately were not observed in $\text{H}\alpha$ by us. Since then two of these, ESO321-G14 and AM1321-304, have been detected by Bouchard et al. (2009), and are included in our Table 3 and subsequent Figures.

Of the dIs that we observed (Table 1), a total of 14 now have measured distances based on the red giant branch tip (Karachentsev et al. 2002, 2007). For the three other dIs we assume a distance equivalent to the mean distance of the Centaurus A Group of 3.8 Mpc, as determined by Karachentsev et al. (2007). In the nearby, southern Sculptor Group of galaxies, it was found that galaxies seem to follow a distance-velocity relationship with very small scatter, defined with the measured distances to nine galaxies (Jerjen et al. 1998), of the form $v_{GSR}(\text{km s}^{-1}) = 119 D(\text{Mpc}) - 136$. It was thus possible to assign a reasonable estimate of distance to a dwarf member based solely on its recessional velocity. Unfortunately no such relationship seems to hold in Centaurus A. In fact, Karachentsev et al. (2007) have plotted over 50 galaxies in the region with both distance estimates (mostly from red giant branch photometry) and recessional velocities, and it appears that there are clearly two subgroups, with one subgroup of dwarfs surrounding Centaurus A with a mean distance of 3.8 Mpc, and the other around M83 at 4.8 Mpc, with no clean distance-velocity relationship. While the Sculptor Group is a loosely bound group with no large disturbance from the Hubble flow, the Centaurus A Group on the other hand seems more evolved, with more complex internal dynamics.

The absolute magnitudes quoted in Table 1 are from the apparent magnitudes observed by Côté (1995), corrected with updated Galactic extinction from Schlegel et al. (1998) and converted to absolute magnitudes using the adopted distances above.

2.2. H α Imaging

The H α images were obtained with the CTIO 0.9m telescope over 8 nights in April 1999. The telescope was equipped with the Tek 2048 CCD, with a readout noise of $3.4 e^-$ and gain of $1 e^- \text{ADU}^{-1}$, and a pixel scale of $0.396'' \text{pixel}^{-1}$. The observations usually consisted of $3 \times 1200 \text{ sec}$ through a narrow-band H α filter centred at 6559 \AA and with a FWHM of 64 \AA , followed by a $2 \times 1200 \text{ sec}$ for continuum off-band images through a filter centred at 6115 \AA and with a FWHM of 140 \AA . R-band images were also acquired (typically 600 sec). The seeing varied between $1''$ and $1.4''$, and the conditions were photometric for 6.5 nights out of 8.

The data reductions were performed mostly with IRAF following the usual procedures. The different images in each filter were registered and then co-added. The co-added off-band image was smoothed with a Gaussian so that in the final image the point-spread functions matched as closely as possible those in the H α image. This continuum image was then scaled appropriately using half a dozen isolated bright stars and then subtracted from the H α image. Figure 1 shows the R images and the final continuum-subtracted H α images. Table 2 lists the positions and fluxes of all the HII regions found in each dwarf galaxy. HST Guide star Reference Frame scans from the STScI Digitized Sky Survey were used to derive accurate positions for the HII regions.

The HII regions are rarely isolated, but are most often located in large complexes and occasionally exhibit complicated morphologies with loops or filaments, which would make it difficult for an automatic procedure to delineate them. Therefore it was necessary to determine the boundaries of each HII region by eye, and, using POLYPHOT, the fluxes were obtained by integrating all the emission within the regions. Each distinct emission peak was defined to be a separate HII region, ensuring that each of them correspond to a separate excitation source. It may be that some of these peaks are just density peaks in the excited gas rather than genuinely separately excited HII regions. In addition, there might be some degree of randomness in the way adjacent HII regions are separated, but these difficulties would also affect regions found by automatic software methods. However, it should be kept in mind that these difficulties will have an influence on the faint-end of the luminosity function of HII regions. When filaments or extended diffuse emission were present, they were included in the most nearby HII regions, since most probably they are ionised by escaping photons from these regions and do not have their own ionising stars. In some cases, some diffuse emission regions were found fairly isolated in the galaxies and, hence, were counted on their own. Most of the sample dwarfs did not have significant diffuse emission, just as the faint dwarfs ($M_B > -15.9$) of Strobel et al. (1991). The borders of the HII regions were set to a constant H α surface brightness level for each galaxy, at our detection limit estimated at about $\sim 3.0 \times 10^{-17} \text{ ergs cm}^{-2} \text{ s}^{-1} \text{ arcsec}^{-2}$. Errors in fluxes are typically around 10%, mostly due to absolute flux calibration uncertainties. No correction for [NII] contamination has been applied to these fluxes; dwarf galaxies are known to have very low nitrogen abundances (see, e.g., Skillman et al. 2003b) so this introduces an additional $\sim 6\%$ flux uncertainty at most. H α luminosities were calculated from the H α fluxes using the distances of Table 1 and assuming a Galactic extinction correction of the form $A(H\alpha) = 2.32E(B - V)$ (Miller & Hodge 1994), with reddening values from Schlegel et al. (1998).

Almost all of our galaxies (except Cen6, UGCA365 and NGC5237) have previous $H\alpha$ measurements in the literature, mostly from the recent survey of Kennicutt et al. (2008). Our fluxes agree within 50% overall with those of this survey. They agree better with those of other authors: IC 4316 and NGC 5408 were imaged in $H\alpha$ by Gallagher & Hunter (1987), who found total fluxes of 1.3 and $34 \times 10^{-13} \text{ erg s}^{-1} \text{ cm}^{-2}$, agreeing well with our total fluxes of 1.2 and $39.2 \times 10^{-13} \text{ erg s}^{-1} \text{ cm}^{-2}$. DDO161 was observed by Meurer et al. (2006) who gives it a SFR of $9.77 \times 10^{-3} M_{\odot} \text{ yr}^{-1}$, very close to our 1×10^{-2} . Finally Kaisin et al. (2007) obtained for UKS1424-460 a SFR of $1.3 \times 10^{-4} M_{\odot} \text{ yr}^{-1}$, again very close to our 1.4×10^{-4} .

3. The HII Regions and the SFRs of the Centaurus A Group dI Galaxies

3.1. The HII Region Distributions and Luminosities

The HII regions in the Centaurus A Group dwarfs are mostly distributed asymmetrically throughout the galaxies, as is seen in the Sculptor Group dwarfs (Skillman et al. 2003a) and other nearby dIs (Brosch et al. 1998; van Zee 2000). This is the case both for the dIs with very little star formation (e.g., ESO 324-G24), as well as the dIs with large numbers of HII regions (e.g., DDO 161). In brighter spiral galaxies, HII regions will most likely be concentrated in the inner parts, and they typically have $H\alpha$ surface brightness profiles similar to broadband V or R surface brightness profiles, peaking in the center Koopmann & Kenney (2006). Our Centaurus A Group dIs have their brightest HII regions most often in the outer parts of the galaxy, sometimes out to the very edge of the optical disk, which is often the case for dIs Brosch et al. (1998). Note that this is true even when accounting for the fact that there is more area at large radii. Only two of the dwarfs have their dominant brightest HII region centred in the nucleus: DDO 161, which is one of the largest dwarfs in the sample, and UKS 1424-460, which has only one HII region. One can see easily from Figure 1 why longslit spectroscopy of dwarfs to estimate their SFRs is rather inefficient, like what is routinely done in surveys at higher redshift. A slit positioned along the major axis of the galaxy would miss the brightest HII regions in many cases, and seriously underestimate the total $H\alpha$ flux for the majority of dwarfs. In some cases (e.g., ESO 324-G24) a slit with a typical slitwidth of 1 arcsec would miss all the HII regions, even if the dwarf was at a distance up to $\sim 250 \text{ Mpc}$ (where $1'' \sim 1 \text{ kpc}$). In fact Perez-Gonzalez et al. (2003) have compared $H\alpha$ fluxes determined by spectroscopy with those measured on $H\alpha$ images for a sample of emission-line objects at a mean redshift $z=0.026$ and found that the spectroscopy yielded fluxes only 1/3 of the total emission-line flux.

Figure 2 is a histogram of the HII region luminosities for all the Centaurus A Group dwarfs. The peak is at roughly $10^{37.4} \text{ erg s}^{-1}$, most of the HII regions being rather low luminosity, which is similar to what is seen for the Sculptor Group dwarfs as well as other nearby dwarfs. The fact that the Centaurus A Group contains on average a significantly larger number of brighter dwarfs than the Sculptor Group (Figure 2) does not translate in a significant differences in the overall HII

regions luminosities distribution. Figure 3 shows the fraction of the total $H\alpha$ luminosity in each galaxy that is contributed by HII regions of a particular luminosity range, ranging from regions with luminosities like that of the Orion nebula $\sim 10^{37}$ erg s $^{-1}$ to supergiant HII regions with $L \geq 10^{39}$ erg s $^{-1}$. Despite the fact that the Centaurus A Group dwarfs contain many more HII regions than those in the Sculptor Group, it appears that the luminosity distributions of these HII regions are very similar for the two groups. The bulk of the HII luminosity in these dwarfs comes from regions with modest luminosities $10^{37} - 10^{38}$ erg s $^{-1}$. The only Centaurus A Group dwarf which contains supergiant HII regions is NGC 5408, classified as a starburst by Kewley et al. (2001), in which Wolf-Rayet features were also detected (Schaerer et al. 1999). The percent contribution from the supergiant regions to its total HII luminosity is just above 70%, which is typical for Blue Compact Dwarfs and starbursts (Youngblood & Hunter 1999). This dearth of supergiant regions in the dwarfs is common, for example in their sample of 29 nearby normal dIs Youngblood & Hunter (1999) found only 2 with supergiant regions. For this reason the fraction of $H\alpha$ emission contributed by all of the dwarfs in the Centaurus A Group compared to that from the main galaxies is negligible: their total contribution comes to less than 1×10^{-11} ergs cm $^{-2}$ s $^{-1}$, which is less than the $H\alpha$ emission from the three largest supergiant regions alone (amongst many) of M83 (Rumstay & Kaufman 1983).

Only two dwarfs out of 19 listed as Centaurus A Group members in Côté et al. (1997) were not detected here in $H\alpha$: UGCA 319 (also known as SGC1259.6-161), and NGC 5206. In the case of the latter this is not surprising, because it is a dE type, classified as T=−3 in the RC3 and T=−2 in Lauberts & Valentijn (1989), with a well-defined $r^{1/4}$ profile (Prugniel et al. 1993). It was not detected in HI (down to $7.8 \times 10^6 M_{\odot}$) and its velocity comes from optical absorption lines measurements (Côté et al. 1997). UGCA 319 on the other hand has now been detected at the Mount Stromlo and Siding Spring 2.3m by Bouchard et al. (2009), with a flux of 1.6×10^{37} erg s $^{-1}$.

3.2. Global Star Formation Rates and Timescales

$H\alpha$ luminosities were converted to current SFRs as in Kennicutt et al. (1994), with:

$$SFR(total) = \frac{L(H\alpha)}{1.26 \times 10^{41} \text{ erg s}^{-1}} M_{\odot} \text{ yr}^{-1} \quad (1)$$

which has been derived for normal spiral galaxies with a Salpeter IMF, and is the conversion adopted by Kennicutt (1998) in his grand synthesis of global SFRs in galaxies. No corrections were made for internal extinction (as had been done for spiral galaxies in Kennicutt 1998) since extinction is normally quite small in these low metallicity systems. A possible exception would be dwarf starbursts, but in their case it is difficult to quantify (see, e.g., Cannon et al. 2003). Adopting a single conversion factor from $H\alpha$ luminosity to SFR for dwarf galaxies which has been derived for normal spiral galaxies certainly carries some uncertainty. One can think of several possible biases, primarily how the IMF might not be universal and/or the production of ionising photons by the stars might be metallicity dependent. It seems indeed that the IMF in low-luminosity galaxies has

fewer massive stars (from a large SDSS study from Hoversten & Glazebrook 2008), either by a steeper slope or lower upper mass cutoff. We nevertheless apply this conversion factor to our dIs for consistency so that our sample can be compared directly to other previous studies which have all used this same factor. One should keep in mind though that SFR levels below about $10^{-3} M_{\odot} \text{ yr}^{-1}$ might be inaccurate, since it seems from simulations that it is at this level that stochastic effects come into play and a depleted upper mass end of the IMF result in a lack of massive stars responsible for H α (Tremonti et al. 2007).

The SFRs listed in Table 3 were calculated using equation (1) with H α luminosities obtained by summing all the HII region luminosities listed in Table 2. Most of these SFRs are very low relative to “normal spiral galaxies”, with values ranging from 3.1×10^{-5} up to $3.4 \times 10^{-2} M_{\odot} \text{ yr}^{-1}$, with the possible exception of NGC 5408 at 8.8×10^{-2} . From the compilation of 150 galaxies of the Local Volume by Karachentsev & Kaisin (2007), spirals have SFRs ranging from 1×10^{-1} up to $5.5 M_{\odot} \text{ yr}^{-1}$. However, these dwarfs SFRs are comparable to the low levels of star formation typical of dIs (typically $1 \times 10^{-3} M_{\odot} \text{ yr}^{-1}$ for a $M_B = -14$ dI in Karachentsev & Kaisin 2007). They are slightly larger on average than those obtained for the Sculptor Group dIs, but this is normal since the SFR is known to be a function of absolute magnitude, and the Centaurus A Group dIs sample includes more brighter dwarfs than the Sculptor Group. In Figure 4 we have plotted the SFRs normalised to L_B versus M_{HI}/L_B , and it can be seen that the Centaurus A Group dIs cover a range comparable to that of the Sculptor Group dIs or the Local Group dIs. What is noticeable in this Figure is that there seems to be a grouping of Centaurus A Group dIs at low M_{HI}/L_B , compared to other dIs. This is probably due to the fact that M_{HI}/L_B scales with absolute magnitude (fainter dwarfs being more HI rich proportionally), and so the brighter Centaurus A Group dIs would have lower M_{HI}/L_B than the average dIs. Indeed, in this group four of the five dIs are among the very brightest dIs of the Centaurus A Group. What also stands out in Figure 4 are the Local Group objects at high SFR/L_B (like NGC 6822 and IC 10). Apparently it is the Local Group dIs which have unusual SFR properties compared with other groups’ dIs. The only dI of the Centaurus A Group that qualifies as a starburst, NGC 5408, is indeed the one with the highest SFR/L_B , at the top end of the distribution. There are no strict definition of starburst on which all astronomers agree, although commonly used denitions are that: a) continued star formation with the current SFR would exhaust the available gas reservoir in much less than a Hubble time; and b) the current star formation normalised by the past averaged SFR is much greater than unity (Gallagher 2005). A definition recently suggested specifically for dwarf starbursts is that their integrated H α equivalent width should be above 100 Å (Lee 2009). NGC 5408 satisfies all of these criteria, and is the only dwarf of the group to do so. It thus seems that the Centaurus A Group dwarf population does not follow the enhanced star forming activity experienced by its larger galaxies. The average SFRs of the dwarfs, as well as the number of dwarf starbursts, are all consistent with what is seen for other nearby dwarfs. Whatever has triggered the star forming episodes of the larger members of the group does not seem to have had any obvious effect on the nearby dIs. With only one dwarf starburst amongst the ~ 30 dIs known in the Centaurus A Group, these numbers are consistent, but on the low side, of what is found overall for nearby dwarfs: Lee (2006) in an 11 Mpc H α

UV survey finds that 6 ± 3 % of low-mass galaxies are currently experiencing a starburst. This is despite the fact that the Centaurus A Group has been carefully combed in HI so that compact HII galaxies would not have been missed, contrary to the field in the 11 Mpc volume.

Table 3 provides two interesting timescales for our dIs to estimate the significance of their SFRs. The first one is τ_{gas} , the gas depletion timescale (= total gas mass/SFR), which is an estimate of the number of years a galaxy may continue to form stars at the current rate until gas depletion. The other one is τ_{form} , the star formation timescale, which is the ratio of the mass of stars present to the current rate of star formation. This provides a rough indication if the galaxy is currently forming stars at a lower or higher rate than it has in the past. Note that τ_{gas} is a lower limit since it does not account for all the material that will be recycled over the course of normal stellar evolution. Despite this, the values of τ_{gas} for the Centaurus A Group dIs are very large, several times the present age of the universe, except for a few particular exceptions. Obviously galaxies which are starbursting will exhibit much shorter gas consumption timescales, and this is the case for NGC 5408. The only other two objects with very short gas depletion times are the two oddest Centaurus A Group’s galaxies: NGC 5237 and ESO 272-G25. NGC 5237, having the appearance of a starburst galaxy but with a nicely elliptical shape, has been morphologically typed from T=−5 (Vorontsov-Vel’Yaminov & Ivanišević 1974) to T=+5 (Prugniel & Heraudeau 1998). Thomson (1992) has suggested that it is the remnant of the spiral which collided with Centaurus A (NGC 5128) and consequently lost half its disk material (creating the ring of gas and dust prevalent in Centaurus A) and that the rest was ejected to form this object out of the dusty, gas-rich remaining disc material. It certainly has many features of early-type dwarfs: in addition to its morphology, its $M_{HI}/L_B=0.17$ is typical of dEs and its color B-I=1.6 (Côté 1995) is the reddest of all the Centaurus A Group dI candidates. On the other hand, it seems to be rotating too fast for a dE and more in line with a dI of this magnitude. No rotation curve is available but the Parkes global HI profile has a width at the 20% level of $\Delta V_{20\%}=89 \text{ km s}^{-1}$ (Côté et al. 1997). It might be indeed that NGC 5237 is undergoing a transformation from stripped late-type spiral to a dE. The other unusual object is ESO 272-G25, classified as ‘peculiar’ by Lauberts (1984). The odd thing about ESO 272-G25 is that it was not detected in HI, down to $7.8 \times 10^6 M_{\odot}$. This is a factor of ~ 5 times lower than what would be expected for a dI of this luminosity. It seems to contain some bright emission knots surrounded by a low surface brightness envelope, reminiscent of some Blue Compact Dwarfs (BCDs). However, BCDs have normal M_{HI}/L_B Huchtmeier et al. (2005). It has several chains of HII regions, and the morphology of the underlying envelope is not dE-type. One might argue that it is a recently stripped dI, but ESO 272-G25 is situated in the periphery of the Centaurus A Group, far from any of the massive members. Another way of making the HI disappear is if the galaxy recently underwent a large burst or several bursts of star formation which would have consumed most the gas available. Normally one would not expect the efficiency to be so high, and besides its SFR/L_B is rather ordinary. ESO 272-G25 is reminiscent of POX 186, another BCD with no HI detected (Begum & Chengalur 2005). In this case, it has been hypothesised that the present burst of star formation has ionised most or all of the cold gas. Both NGC5237 and ESO272-G25 would need some dedicated follow-up observations to understand their true nature.

Figure 5 shows histograms of τ_{gas} for the Centaurus A Group dIs compared to the Sculptor Group dIs (Skillman et al. 2003a), the Local Group dIs (Mateo 1998), and the large sample of isolated dIs from van Zee (2001). It is the norm for dIs to have large values of τ_{gas} . In comparison the large sample of spirals of Kennicutt et al. (1994) have a mean τ_{gas} of 3.6 Gyr ($\log(\tau_{gas})=9.6$). It thus appears that dIs can continue to form stars with their current level of low SFRs in a continuous manner for several Hubble times without running out of fuel. Kennicutt et al. (1994) pointed out that in calculating τ_{gas} the total gas mass detected in the galaxy is used when in fact one might want to consider only the gas within the optical radius of the galaxy, which would be effectively available for star formation. Only a handful of dwarfs here have HI aperture synthesis data such that this could be evaluated, but it turns out that from the HI radial surface density profiles of Côté et al. (2000) the extended gas represent only between 5 to 10% of the total HI mass, because the gas profiles drop off sharply beyond the optical edge. All of the dIs in Figure 5 had values of τ_{gas} calculated in the same way, using all the gas, for comparison purposes. It appears that the Centaurus A Group dIs and the Sculptor Group dIs have a similar distribution of τ_{gas} , and that it is the Local Group dIs that have a different distribution, with fewer galaxies with long τ_{gas} which could continue to form stars at the present rate for a long time, and more galaxies at small τ_{gas} which will be depleted soon.

The same thing is seen in the histograms of the star formation timescales τ_{form} for these same groups of dIs (Figure 6). The values of τ_{form} calculated here are just rough estimates; what one really would want to evaluate is the ratio of the past average SFR to the current SFR. However, to calculate the past average SFR one would need to know the mass of stars formed over the lifetime of the galaxy. This means some assumptions need to be made about the mass-to-light ratio of the stellar material, and also about the age of the galaxy. We have derived our estimates following the simplification of Hodge (1993), who simply adopts a mass-to-light ratio of one (which makes sense for typical colours of dIs). With $M/L = 1$, τ_{form} becomes simply equal to L_B/SFR . In Figure 6, similarly to Figure 5, the Centaurus A Group dIs and Sculptor Group dIs follow the same distribution while the Local Group dIs distribution stands out, with more dIs with short τ_{form} , again because of the higher number of dIs starbursting or forming stars at a much higher rate than they have in the past. Using the Kennicutt (1983) sample of galaxies, Hodge (1993) obtained average τ_{form} values of 60 Gyr for early-type spirals, 15 Gyr for late-type spirals, and 8 Gyr for irregulars. Here the dIs of nearby groups have slightly longer τ_{form} , which means that they have lower current SFRs, about sufficient to build the current stellar population over a Hubble time.

A more direct way of evaluating the star formation history of a galaxy is through color-magnitude diagrams (CMD) of their resolved stellar populations. The numbers of stars in different regions of the CMD (main sequence, red giant branch, etc.) can be used to retrace the star formation history. CMDs of many of the Centaurus A Group dIs were built from HST/WFPC2 data by Karachentsev et al. (2002). Unfortunately the data are mostly too shallow for in-depth star formation history reconstruction (their goal was to determine distances using the tip of the red giant branch). One can distinguish in most of the dIs a main sequence indicating recent star

formation, as well as an important intermediate age component, which is at least compatible with deep CMDs obtained for Local Group dIs (e.g., Dohm-Palmer et al. 1998), showing that, except for a few starburst dwarfs, star formation has occurred not in (a few) big bursts but rather in a continuous stochastic manner, with slow and steady star formation through time with some periods with a slightly more elevated rate (by a factor of only a few).

4. Star Formation Trends in dIs

The Centaurus A Group dwarfs show a very wide range of SFRs, as seen from Table 3, even when scaling by the luminosity, as in Figure 4. The SFR/L_B in Centaurus A Group dIs and other local dIs range roughly from $\sim 10^{-12}$ to $10^{-8} M_\odot \text{ yr}^{-1} L_\odot^{-1}$, overlapping with that of normal spirals which have typically $\text{SFR}/L_B \sim 10^{-9} M_\odot \text{ yr}^{-1} L_\odot^{-1}$. One then must wonder if the star formation activity of a particular galaxy really depends in any way on some of its global properties, such as gas-richness, color etc. (§4.1). In §4.2 we will look into the local conditions that seem necessary for star formation to take place, and then in §4.3 we will inspect if the star formation activity is perhaps more dependent on the environment in which the dwarf galaxies are located, both locally and globally. §4.4 will discuss the morphology-density relation in the group, and §4.5 will offer a global comparison between the Centaurus A Group and the Local and Sculptor Groups.

4.1. SFR Dependence on Global Properties

We will investigate here if the SFRs correlate in any way with some global parameter of the galaxies, such as magnitude, central surface brightness, color or HI content, as was done in Hunter et al. (1982), van Zee (2001) and Hunter & Elmegreen (2004). To look at how SFRs might depend on these global parameters, one must first somehow normalise these rates to some measure of the size of the galaxy -since obviously larger galaxies have a larger volume to harbour HII regions. One may think then that the best normalisation should be achieved by looking at SFR per unit mass of the galaxy. As a measure of the mass, one can use a) the total baryonic mass, e.g., the mass in stars and gas, or b) the total dynamical mass. The difficulty with the first option is that, although all the dIs in the sample have good HI mass estimates, the mass of their stellar disk can only be estimated approximately because of the unknown mass-to-light ratio for the stellar material (at best, some estimates could be obtained using the color indexes of the galaxies, e.g., Lee et al. 2006). The second option is not much better, since to calculate the dynamical mass $M_{dyn} = RV_{rot}^2/G$, one needs the rotation velocity of the dI. Some of the dIs in our sample have been mapped in HI with aperture synthesis and have reliable rotation curves so these V_{rot} are known with some accuracy. But for the majority of the sample only estimates of V_{rot} are available based on single-dish HI width measurements and rough inclination angles (and M_{dyn} is inversely proportional to $(\sin i)^2$). For these reasons it is safer to normalise the SFRs to some sort of measure of the area of the galaxy. Hunter & Gallagher (1986) chose to use the Holmberg radius (the radius at which $\mu_B=26.6$ mag

arcsec⁻²) for their sample of Irregular galaxies. However, our sample is composed entirely of dIs that are typically of lower surface-brightness (in fact, on average, surface brightness correlates with size). The choice of the Holmberg radius is therefore not appropriate, as the lowest surface brightness dwarfs profiles will reach the Holmberg radius much sooner. Consequently a unit in terms of the luminosity exponential profile scalelength is chosen, and the final normalisation adopted is an area calculated as $\pi(1.5\alpha)^2$ (the Holmberg radius corresponding roughly to 1.5α for our range of dwarfs).

In Figure 7, SFR/area is plotted against several global properties: the absolute Blue Magnitude, the B central surface brightness, the HI mass to luminosity ratio M_{HI}/L_B , and the color $B - R$. No clear correlations are present for any of these parameters, confirming the results of previous studies, e.g. van Zee (2001) and Hunter & Elmegreen (2004). The normalised SFR versus the surface brightness shows at best a hint of a correlation, but this is not surprising, as an enhanced SFR would bring as a normal consequence the brightening of the surface brightness. There is also a hint of a trend for lower luminosity galaxies to have lower SFR, but the scatter is very large in SFR. There is no trend between SFR and colours (B-R), even though bluer colours are a sign of a stellar population with a younger mean age. For our set of dwarfs it is therefore not a global galaxian parameter that clearly influences the strength of the star formation in a given object. It is perhaps more likely that it is the local conditions that are determining the level of star formation activity in the galaxy.

4.2. SFR Dependence on Local Conditions

It has been observed in numerous dIs that the majority of their HII regions, especially the brightest ones, seem to be associated with local peaks in the HI distribution, most often being located along ridges of regions of higher HI column densities. In spiral galaxies star formation seems largely regulated by the propagating spiral density waves, but dIs, except for the largest ones, do not have the required gravitational potentials to support these. Successful star formation ‘laws’ have been devised for spirals, relating locally the star formation rate to a power of the gas density, such as in the ‘Schmidt law’, or the now more popular Kennicutt (1998) version. Moreover there is good evidence that there exists some threshold below which the star formation plummets abruptly. The Toomre (1964) dynamical threshold (see also Kennicutt 1989) is based on the idea that there should be a critical surface density above which a self-gravitating infinitely thin rotating gas disk is locally unstable to axisymmetric perturbations; this critical surface density being proportional to the gas velocity dispersion and the epicyclic frequency. However, it has often been observed in dIs that their gas densities are well below their threshold for star formation across the entire galaxy, and yet they contain many star forming regions.

It has been suggested that observations could be explained instead by a star formation rate dependence on gas volume density (rather than surface density), which diminishes drastically in the outer disk due to the vertical flaring of the gas layer, and this would remove the need for a large-scale gravitational threshold (Ferguson 2002). DIs’ star-forming properties might be difficult to explain

with this scenario though, as they are more puffy than larger spirals, and have proportionally more flaring, so one would expect lower SFRs throughout the dwarf compared to a spiral judging by the gas surface density, which is contrary to the observations that dwarfs observed SFRs are much higher than predicted. In dIs, regions of high SFRs are popping everywhere in the galaxy, very often at larger radii while none are observed in the central regions. Therefore the argument of gas 'dilution' as the gas envelope flares at larger radii and therefore the gas volume density lowers does not agree well with the observed SFRs. The newly proposed model of thermo-gravitational instability of Schaye (2004) is a promising alternative. According to Schaye (2004) the UV background radiation implies a surface density threshold for the formation of a cold gas phase (and this threshold agrees with the observed one). The transition to a cold phase, associated with a drop in the pressure, triggers gravitational instabilities and hence star formation. For gas densities below the threshold, self-gravitating gas clouds are kept warm and stable by the UV background radiation. However, it seems that somehow there must be a feedback between the energy injected in the ISM (through SN, stellar winds etc) and the ISM itself to regulate the star formation in dIs. Hirashita (2000) argues that the heating (from stellar feedback) must be very efficient in dIs because of their small size, and on the other hand the cooling does not become effective because of their low metallicity abundances. With the balance of these two processes the intermittent star formation activity of small-size dIs can then be reproduced.

Looking at the sample of Centaurus A Group dwarfs addressed here, only five dwarfs have been properly mapped in HI by aperture synthesis: ESO 381-G020, DDO 161, ESO 444-G084 and ESO 325-G011 from Côté et al. (2000); and IC 4316 from de Blok et al. (2002), all done with the ATCA. Those first four dwarfs all have gas surface densities lying well below the critical density for star formation (calculated following Kennicutt 1989) as shown in Côté et al. (2000). Despite this they all harbour numerous star formation regions as we have seen above. In each case the HII regions are found to be contiguous with the HI density peak or circling very closely the region of the HI peak, as is often observed in dwarf galaxies (e.g., Skillman et al. 1988; Taylor et al. 1994). When there are two distinct separate HI peaks, the bright HII regions are even seen in two clusters, surrounding each of the peaks. This is similar to what was seen in the dwarf galaxies of van Zee et al. (1997a), see in particular UGC5764 in their Figure 11. In each of these four dwarfs it is found that the sites where current star formation activity is taking place are always in regions where the HI gas column density is at least 7.3×10^{20} atoms cm^{-2} (including all outlying HII regions, down to our detection limit). And the brightest HII regions in each dwarf are limited to regions of over 9.8×10^{20} atoms cm^{-2} . For IC 4316 it is found that the HII regions lie within the contour of the 2×10^{20} atoms cm^{-2} level, however the spatial resolution for the IC 4316 data is twice that of the Côté et al. (2000) data, with a synthesised beam corresponding to about 1 kpc at the distance of the dwarfs. Conversely regions with HI gas column density of at least 7.3×10^{20} atoms cm^{-2} do not necessarily exhibit fresh HII regions, so this level of gas surface density seems like a necessary condition for active star formation in dwarfs but is not the sole one. Since these regions are very much near the central parts of the galaxies it is unlikely that there are large volume density variations due to e.g., flaring in these parts of the galaxies. It thus seems that a simple gas volume density limit is not

sufficient to explain star formation activity. However in the inner parts of the galaxies one does not know the detailed heating processes and the exact locations where the stellar events have occurred which will have influenced the temperature and density of the gas. On the other hand the cooling rate, dependent on the metallicity, should be fairly uniform across the dwarf, since the metallicity does not show strong gradients in cases where several HII regions were measured in the same object. It is thus very possible that the balance of the two, heating and cooling, indeed produces the star formation activity observed. Note that in dwarf galaxies it is very probable that there is still, as in larger galaxies, some low level of star formation beyond these thresholds, as can be traced now in the UV ((Boissier et al. 2007)). These thresholds seem to be where H_α is no longer detected because the number of massive stars ($M > 10M_\odot$) with large ionizing fluxes responsible for it are rapidly dwindling, while the UV continuum emitted by slightly smaller, longer lived stars can still be observed.

4.3. SFR Dependence on Environment

There are many reasons to suspect that a dwarf galaxy’s local environment might play a role in increasing/decreasing its star formation. Depending on the local galaxy density, e.g., if the dwarf is rather isolated or in a group or in the middle of a cluster, various processes are expected to affect its star formation. Star formation might first be induced as a dwarf starts approaching the cluster centre, due to the pressure in the intracluster medium leading to compression of gas clouds, or cloud-cloud collisions (Elmegreen 1997). Then ram-pressure stripping might remove its reservoir of gas, therefore halting its star formation activity. Strangulation, where hot gas is depleted from the dwarf’s halo after it enters a hot medium (which means no more hot gas can cool and eventually form new stars) is another possibility (Larson et al. 1980). It has been argued though that these processes are unlikely to be very effective in a group environment: a) the pressure force for the stripping depends on the square of velocity dispersion of the group and these are too low in groups ($\sigma < 400 \text{ km s}^{-1}$) to produce a significant effect; b) strangulation is a slow process, which takes ~ 1 Gyr in clusters, and moreover it requires an intracluster medium (Conselice 2006). Galaxy-galaxy interactions, on the other hand, are frequent in groups, and this is a process that should induce star formation in the participating galaxies, should they be mergers or just low velocity interactions.

Hunter & Elmegreen (2004) investigated how the SFRs of galaxies depend on their proximity to other galaxies, and found no correlation in their sample of 94 nearby galaxies. However the distances used for the galaxies were for the great majority only estimated from Hubble’s law. Even in superclusters, like Virgo and Coma, Gavazzi et al. (1998, 2002) found that the star formation rate for late-type galaxies are the same as in the field. They found decreasing SFRs with decreasing distance from the cluster centre only for bright galaxies, but not for the dwarf galaxies. In compact groups too Iglesias-Páramo & Vílchez (1999) found the same median SFRs in the middle of the groups compared to the field for their sample of disk galaxies.

In Figure 8 we explore how the SFRs of our dIs vary depending on the dwarf’s distance to

the nearest spiral galaxy. Only the Centaurus A Group dIs for which there is an accurate distance measurement were used, and ESO 223-G09 was excluded too because at a distance of 6.4 Mpc it has to be considered a background object. The plot show the normalised SFR/area versus the distance of the dwarf to the nearest large galaxy of the group. As expected, there is no correlation, either for the Centaurus A Group dIs, or for the combined sample with the Sculptor Group dIs and the Local Group dIs. Similarly, if one looks at the SFR/area versus the distance to the group centre there is no apparent trend. It thus appears at first sight that the star formation activity of a dI in nearby groups does not depend on its immediate local environment. However the existence of a morphology-density relation in both the Local Group and the Sculptor Group ((Skillman et al. 2003a)) points to some underlying environmental effects at play, and below we take a look at the situation in the Centaurus A Group.

4.4. The Morphology-Density Relation for the Centaurus A Group Dwarf Galaxies

Cluster galaxies have long been known to follow a morphology-density relation, where early-type galaxies (including early-type dwarf galaxies) are predominantly found in the higher density regions of the cluster whereas the late-type and irregular galaxies are in the periphery in lower density regions. This morphology-density relation is also found to work in the Local Group, in which faint dSphs and dEs are found predominantly in the vicinity of the Milky Way and M31 while dIs are widely spread in the group (van den Bergh 1994a). This is also true in the nearby Sculptor Group, where the majority of the dwarfs now have good distance estimates and therefore a 3D picture of the group is possible, and there too one finds the early-type dwarfs at a mean distance of only 0.22 ± 0.21 Mpc from the nearest spiral galaxy while dIs are at a mean distance of 0.95 ± 0.61 Mpc (Skillman et al. 2003a). Interestingly, the so-called ‘transition’ dwarf galaxies, objects that show characteristics of both dEs and dIs, are found at intermediate distances, with a mean distance of 0.50 ± 0.34 Mpc to the nearest (large) spiral galaxy (Skillman et al. 2003a). Naturally, one is then led to think that there are probably some environmental effects at play which are able to drive a normal dI into a transformation into a dE/dSph, as the dI falls into the group potential. Possible such effects include ram-pressure stripping (Gunn & Gott 1972), galaxy harassment, which transforms a small disk galaxy into a left-over dE or dSph (Moore et al. 1996), or tidal stirring, where repeated tidal shocks partially strip the halo and disk of a dI and reshape it into a dE/dSph (Mayer et al. 2001a,b). If all dIs are rotationally supported and dSphs are not (although there is mounting evidence that this is not strictly true, e.g., De Rijcke et al. 2004; Geha et al. 2006), then it takes more than just gas removal to convert a dI to a dSph, since some loss of angular momentum must also occur. This means that internal mechanisms of gas removal, such as gas expulsion through galactic winds, or gas exhaustion through continued star formation, are not sufficient, and other processes are needed. Furthermore, one would normally expect to find gas return from dying stars collecting with time in dSphs, with a return rate thought to be 1% to 5% of the stellar mass. Nonetheless, dSphs have extremely low HI non-detection limits which are well below the expected gas mass. This means some other processes must be at play to remove this

gas.

To investigate the morphology-density relation in the Centaurus A Group, first the criteria to classify a dwarf as a ‘transition’ dwarf need to be clarified. For Sandage & Hoffman (1991) the definition of a ‘transition’ dwarf was based only on its optical appearances, and any dwarf exhibiting any characteristics belonging to the other group would be classified as a ‘transition’ dwarf. This, of course, produced a very heterogeneous set of objects (Knezek et al. 1999). Sandage & Binggeli (1984) introduced a dS0 class, again based purely on visual inspection, but they correctly inferred that these dwarfs must have a disk component. Indeed, e.g., Aguerri et al. (2005) showed that dS0s need a Sersic + exponential fit to their luminosity profile. In their study of dwarfs in the Virgo cluster Lisker et al. (2006) creates a new class dEdi to include all dEs with embedded disk features (hence including the dS0s). However, it seems that disks are so common amongst dEs that they should be considered a normal feature for an early-type, very much like for the bright Elliptical galaxies which often come with nuclear disks too ?, even for systems which are otherwise apparently ‘normal’. Similarly, the presence of HI gas in a dE should not be a sufficient criterion to classify it as a transition object. Conselice et al. (2003) find that about 15% of Virgo dE are detected in HI, and again this is similar to the detection rate of big Ellipticals, detected in HI by HIPASS at a rate of 5% for Es and 12% for S0s (Sadler 2001). Many ‘normal’ nearby dEs are known to have some HI (e.g., NGC 205, NGC 185 in the Local Group), although typically dIs have $\geq 10^6 M_{\odot}$ while dEs and dSphs have $< 10^5 M_{\odot}$.

Here we will adopt the definition of ‘transition’ dwarf following Mateo (1998), Skillman et al. (2003a), and Grebel et al. (2003), where such a dwarf should have cold gas but no active star formation, in other words it is detected in HI but not at all in $H\alpha$ or with an abnormally faint flux. They represent gas-rich examples of dSphs, and indeed they are found to fall in the luminosity-metallicity relation near the dSph locus rather than the dI one (Mateo 1998). This still is not a clear-cut way of differentiating these objects as there appears to be a continuum of dwarfs from dEs to dIs with various amounts of $H\alpha$ and HI. Normal dIs, according to the star formation histories constructed from their resolved stellar content, are continuously forming stars at a low level, until they get into a burst episode every few Gyrs. The presence or absence of just a few HII regions will then determine if the object at this point of time get classified as a normal dI or a transition dwarf. The transition dwarfs defined this way will inevitably be still a little bit of a mixed collection of objects, with objects who have truly halted all their star formation activity by depletion of enough gas, and those that have still enough gas but are simply in-between such episodes of star formation. Note though that for nearby dwarfs like in our sample here, sometimes only one hot star in the galaxy is sufficient to enable its detection in $H\alpha$. For example in Pegasus, there are only 2 small HII regions detected (Skillman et al. 1997). Despite these detections it has been classified a transition dwarf by (Mateo 1998), because the $H\alpha$ flux is extremely faint and its τ_{gas} is enormous ($=3220$ Gyr). In fact, star forming galaxies follow a trend of increasing SFRs with decreasing (brighter) magnitudes, equivalent to a close to constant star formation rate per unit luminosity (see Figure 2 of Karachentsev & Kaisin 2007), but Pegasus, and other transition dwarfs with detected $H\alpha$ fluxes,

falls completely off this trend found for all others dIs and spirals.

Following these criteria for defining transition dwarfs, there is a total of four transition dwarfs in the Centaurus A Group: ESO 269-G58, UGCA 365, ESO 384-G016, and UKS 1424-460. UGCA 365 has one HII region but its τ_{form} is enormous (= 1422 Gyr); and UKS 1424-146 is also detected in H α here but it is only an extended diffuse region, with no obvious ionising source, and its τ_{form} is high (= 281 Gyr). Both ESO 269-G58 and ESO 384-G016 are detected in HI, and have H α detections in the literature which are very low compared to dwarfs of their magnitude. These transition dwarfs add to the five cases in the Sculptor Group: SDIG, DDO 6, UGCA 438 (see Skillman et al. 2003a), ESO 294-G10 (Jerjen et al. 1998; Bouchard et al. 2009), and ESO 540-G32 (da Costa et al. 2007); and six in the Local Group: LGS3, Antlia, DDO 210, Pegasus, Phoenix (Mateo 1998), and the recently discovered Leo T (Irwin et al. 2007).

Using only the Centaurus A Group dwarfs with known distances (see Karachentsev et al. 2007), the distances to the nearest large galaxy in the group for dwarfs of the three types (dI, transition and dE/dSph) are plotted in Figure 9. The Centaurus A Group dwarfs reinforce the trend that is seen in the Local Group and Sculptor Group, where dIs are found at a much larger mean distance from a massive galaxy than the dEs and dSphs. Overall, for the three groups, dIs are at a distance of 0.85 ± 0.55 Mpc (1 σ standard deviation), while dEs and dSphs are at 0.23 ± 0.20 Mpc. Interestingly, the transition dwarfs are found right in the middle at 0.54 ± 0.31 Mpc. Kolmogorov-Smirnov tests to determine the significance of the differences between the three distributions indicate that indeed all three distributions are significantly different. The probability that the transition galaxies come from the same sample as the dIs is only 3%. The probability is even lower, less than 1%, for the transition galaxies to come from the dEs. This is mostly due to the strong peak at ~ 150 kpc in the dEs distributions, as the vast majority of dEs and dSphs (all but two) are satellites of the massive radio galaxy Centaurus A. The low average distance for dEs and dSphs might be biased by the fact that many targeted searches have been done around bright galaxies, e.g., M31, and therefore will necessarily find mostly close-by dSphs at small angular separation (although only about half of all the Andromeda dSphs have been included in the Figure since the rest do not yet have good distance estimates). For the Centaurus A and Sculptor groups, no such bias should apply, as most of the dEs and dSphs were found in all-sky searches on POSSII and ESO/SERC plates for nearby dwarf galaxy candidates (e.g., Karachentseva & Karachentsev 1998; Karachentseva & Karachentsev 2000), which were not restricted to particular narrow group region. Moreover, for the transition dwarfs and normal dIs, deep HI scans were done with HIPASS (Banks et al. 1999) over the entire group regions, so the objects at the periphery of the groups would have had the same chance of being detected as those nearer the center of the group.

The fact that the mean distance of the transition dwarfs to the nearest massive galaxy is quite large, 0.54 ± 0.31 Mpc, poses some difficulties for most of the proposed scenarios for the transformation of dIs into dSphs. For example, simulations of gas-dominated dwarf galaxies transforming via the combination of ram pressure and tidal stripping (Mayer et al. 2006, 2007) successfully produce dSphs with properties compatible with observations. However, in this scenario, the original

gas-rich dwarf needs to go through repeated tidal shocks at the pericenter of its orbit, over a time period of about 10 Gyr, each orbit lasting a few Gyrs, and with apocenters significantly smaller than 0.5 Mpc (although in simulations some occasional extreme satellites on nearly radial orbits can have apocenters far exceeding the virial radius of the primary galaxy). It thus seems unlikely that our transition dwarfs are in the middle of this process, being too far from their primary galaxy. In fact, many might even be infalling into the group potential for the first time (as shown for the Local Group with orbit tracing by Peebles 1989). The crossing times of these groups are several Gyrs, and for Sculptor it is even more than half a hubble time at 6.6 Gyr (Karachentsev 2005).

Moreover, simulations show that at the first tidal shock a strong bar instability is created, which funnels the gas into the central few kpcs, producing bursts of star formation. This is not seen in our transition dwarfs, which do not show more striking bar features than normal dIs. Note that the Mayer et al. (2006, 2007) simulations were carried out on gas-rich dwarfs with NFW halo profiles, while tidal and ram pressure stripping would be much more effective and quicker on a flat core dwarf (which we would argue to correspond better to the observations in any case, e.g., Côté et al. 2000). Similarly, the galaxy harassment scenario is unlikely to have produced the transition galaxies observed here. Although, in this case, the large distance of the dwarfs to a main galaxy is not problematic (in the Moore et al. 1996, simulations the greatest harassment was obtained for galaxies on elongated orbits with apocenters typically of 600 kpc), the effect of the high-speed close encounter is clearly visible on the galaxy’s morphology after the very first encounter. This first encounter produces severely disturbed barred spirals, with sharp and dramatic features, such as tails and rings (Moore et al. 1996). It takes several encounters before the galaxy shapes itself into a prolate figure, flattened equally by rotation and random motions. The nearby transition dwarfs do not show such features. Rather, many exhibit a morphology similar to post-starburst objects, with a large higher surface brightness region where presumably elevated star formation has last occurred.

It has been assumed so far that the observed transition dwarfs might indeed be in some intermediate phase between gas-rich dwarf and dSph. But one might argue that, since dIs are constantly going on and off with their star forming activity, that these so-called transition dwarfs might just be completely normal dIs that happen to be at the extreme tail of low SFRs amongst quiescent dIs. But one would then have to explain why the ‘transition’ dwarfs are found to have a smaller distance on average to their primary galaxy compared to normal dIs. The natural explanation would be that their quiescent period and SF bursts are somehow linked to their positions in their orbits, with star formation being mostly triggered at each pericenter passing (such that the dwarfs that we classify as transitions have just gone through a burst and are now in a post-starburst phase with no more active SF). But if this were truly the case, then one would expect to see a similar correlation between the SFRs, normalised by the area, and the distance to the primary galaxy for *all* dIs, as they would be expected to be affected the same way along their orbits. But no trend is found in Figure 8. In view of their smaller average distance to their primary, it is therefore difficult to see the transition dwarfs as nothing more than hyperquiescent dwarfs.

The fact that the transition dwarfs are found closer in the groups than on average other dIs points to an underlying cause related to the group environment. Something, or some combination of effects, must be acting on them, with the final outcome being gas depletion and hence the end of star formation in the galaxy. Whatever these effects are (stripping, stirring, harassment etc.), the first signs of it should be visible on the gas envelope of the galaxy, the gas being the galaxy’s component most vulnerable to stripping, ejecting, accreting, or funnelling etc. In fact, in the Virgo Cluster, Chung et al. (2007) find galaxies with long HI tails due to ram pressure stripping and/or tidal interactions, and it appears that these galaxies begin to lose their gas already at intermediate distances from M87 (0.6 to 1 Mpc), similar to the distances of our transition dwarfs to their primary galaxy. In a group environment too, as the normal dIs fall into the group potential perhaps then some signs should start to show up in their HI envelope as they get closer to the primary galaxies. One might then think, since the transition dwarfs typically have less gas than normal dIs Skillman (1996), that perhaps there is a similar trend in normal dIs, with those at large distances from the group’s primary galaxies being the most gas-rich and those closer in being gas poorer. Figure 10 explores this possibility, where the HI mass to light ratio M_{HI}/L is plotted against the distance of each dwarf from a group’s primary galaxy. There is no such trend visible. DIs’ HI content therefore does not seem to be depleted slowly as the dIs approach closer to their primary galaxy, on the way to start their transition. Perhaps what one should be looking for is not a decrease in total HI mass, but rather a lowering of the HI gas surface densities, as they are closely linked to star formation thresholds (see previous section). Any changes in the average HI surface densities could result in influencing the star formation rate of the dwarf galaxy.

Unfortunately, it is very difficult, with existing data, to study quantitatively any major differences between HI surface densities of transition dwarfs and dIs, as well as between dIs further or closer to the group’s galaxies, because the few dwarfs which have been imaged in radio with aperture synthesis all have been observed at different spatial resolutions with different beam sizes. Hence, a dwarf might have an HI peak just as strong as the others, but if it is observed at lower resolution with a larger beam the signal will be diluted and the peak HI column density will be underestimated. From the sparse data which are available, it does appear that dIs do not show dramatic variations in their HI surface densities depending on their positions in the groups, although there is a hint that transition dwarfs do have lower average HI surface densities. For example, for the eight Sculptor Group and Centaurus A Group dwarfs imaged in HI by Côté et al. (2000) with roughly the same beamsizes, the only transition dwarf in this sample, SDIG, also happens to have the lowest HI surface densities. Lo et al. (1993) pointed out that LGS3 also has HI column densities 1/10th those of all the other 9 nearby dIs in their sample. There are several transition dwarfs though (e.g., Pegasus, DDO 210 from the Local Group), that have very high peak HI column densities, much higher than the levels at which there is star formation in many dIs. In any case, the HI distribution does not seem to corroborate many of the proposed scenarios for the transition from dI to dSph, which often involves as a first step the HI being funnelled through a strong bar to the centre of the dwarf. The HI loss and its consequence the end of star formation must probably happen on a very short timescale as the dI falls into the group core, or its orbit gets closer to larger

galaxies.

4.5. Comparison with the Local Group and Sculptor Group

The Centaurus A Group is now one of the only nearby groups at < 5 Mpc which have had its dwarf galaxies thoroughly surveyed in $H\alpha$, along with the Sculptor Group (Skillman et al. 2003a), and the Local Group (see Mateo 1998, review). This gives us the chance to compare for the first time the star forming properties of dwarfs in different group environments.

Looking through Figures 3 to 10, we can make the following comparisons between the three groups. Firstly, it appears that the Local Group dwarfs have on average a lower HI mass to light ratio M_{HI}/L , compared to the Centaurus A Group dwarfs, and especially the Sculptor Group dwarfs, which contain several objects having M_{HI}/L above 2. The Local Group lacks these very gas-rich dwarfs.

Second, from the SFR/L_B from Figure 5 and $SFR/area$ of Figure 9, it appears that the Local Group is notably different from the two others in its higher number of dwarf galaxies with high SFRs. Indeed, the Local Group is rich in dwarfs with presently elevated normalised SFRs, such as IC 10 or NGC 6822, which are rarer in other groups. These dwarfs are not necessarily classifiable as starbursts, but they nevertheless have SFRs much higher than the average SFR for a dwarf of the same luminosity and/or HI mass (typically $\sim 1 \times 10^{-2} M_{\odot}yr^{-1}$). One might have expected the Centaurus A Group to have the largest number of starbursting and/or high star-forming dwarf galaxies, considering that all the main members of this group show signs of activity or recent activity. However, it appears that the dwarf population of the group does not follow the trend set by the larger galaxies.

The Centaurus A Group is also the densest of the three groups. One might think that its dwarfs may have simply evolved much faster than the main members, and that their active periods are in the past, with many dwarfs having already achieved a successful conversion from dI to dSph/dE, while this process is still more actively taking place in the two other groups. If this were the case, then detailed star formation histories of dIs and transition dwarfs should show differences between the Centaurus A Group and the other two groups' dwarfs. However, detailed HST CMDs for three dIs of the group by Grossi et al. (2007) finds that their SFRs have been very low, except perhaps for one object (HIPASSJ1321-31) which has a peculiar red plume suggesting a ‘miniburst’ about 300 to 500 Myr ago. In the Local Group, where most of the dIs have high quality CMDs, the clearest conclusion that can be drawn from these CMDs is that no two dIs have the same star formation history. The five transition dwarfs in particular do not show any recent spike of star forming activity, except perhaps Antlia in its inner regions only. If it is truly a burst of star formation which has triggered the process of transformation in these dwarfs from dI to dSph, then these bursts must have happened many Gyrs ago, as age indicators from CMDs lose resolution for ages exceeding a couple of Gyrs. All three Groups show more or less similar numbers proportionally of transition

dwarfs: six for the Local Group, four for the Centaurus A Group, and five for the Sculptor Group. So the process of transformation of dIs into dSph, or at least into transition dwarfs, has the same efficiency in all groups, and the timescales to go through this process are probably similar too.

It is surprising to see that it is the Local Group which has the dwarfs with the highest HI mass to light ratios, and the largest number of dwarfs with high SFRs. When looking at the basic properties of the groups, the Local Group has, for example, a crossing time and a density of galaxies similar to those of the Centaurus A Group, while the Sculptor Group has a considerably longer crossing time and lower density. The Local Group also has a very average total mass in galaxies compared to the Centaurus A Group and the Sculptor Group, as well as an average mass to light ratio as a whole (Karachentsev 2005). The number of transition dwarfs are all proportionally similar (all this within small numbers statistics), while one might have expected this number to scale with the crossing times and density of galaxies in the group, since according to the transition scenarios one needs the dIs to be on closer orbits with a main galaxy for the various effects to be effective. The transition dwarf phase therefore seems a widespread phenomena in a wide variety of group environment.

5. Conclusions and Summary

From our H α imaging survey of dIs in the Centaurus A Group, we find the following results:

The Centaurus A Group dIs do not have enhanced star forming activities, and do not contain a larger fraction of dwarf starbursts when compared to other nearby groups such as the Sculptor Group or the Local Group. This is perhaps surprising given that all large galaxies in the group are exhibiting or have recently exhibited a period of enhanced star formation. The gas depletion timescales of the dIs are very large, and except for a few rare cases, are several times the present age of the universe.

We find that the SFRs of the Centaurus A Group dIs do not depend on any global properties of the galaxies, such as magnitude, central surface brightness, HI mass-to-light ratio, or B-R color. They do not depend on local environment either, in particular there is no correlation with the distance of the dI to the nearest large galaxy of the group.

Nonetheless, there is a morphology-density relation in the Centaurus A Group, similarly to the Sculptor Group and Local Group, in the sense that dEs/dSphs tend to be at small distances from the more massive galaxies of the group, while dIs are on average at larger distances. Interestingly, the four transition dwarfs of the Centaurus A Group (ESO 269-G58, UGCA 365, ESO 384-G16 and UKS 1424-460) have an average distance intermediate between those of the dEs/dSphs and dIs. Together with the four transition dwarfs of the Sculptor Group and six of the Local Group, they have a quite large average distance of 0.54 ± 0.31 Mpc. This large distance poses some difficulty for the most popular scenarios proposed for transforming a dI into a dE/dSph. Both ram-pressure with tidal stripping, as well as galaxy harassment, need the dI to be much closer in its orbit to the

large galaxy to have any effect. Also, after the first encounter, they produce transition objects that appear as strongly barred disturbed objects. If the observed transition dwarfs are indeed missing links between dIs and dE/dSphs they are unlikely to have been produced by these mechanisms.

A possible scenario is that the IGM in these groups of galaxies is inhomogeneous, with regions of higher densities $> 10^{-5} \text{ cm}^{-3}$, where clumps would be able to remove the HI from a dI by ram-pressure stripping. Several observations point indeed towards such a possibility. According to hydrodynamical simulations most low-redshift baryons are expected to be found in a warm-hot intergalactic medium (WHIM). This WHIM has already been detected in clusters of galaxies, e.g. Takei et al. (2007). In groups of galaxies too, OVI absorption lines studies in the UV (Sembach et al. 2003) and X-ray absorption lines studies (Nicastro et al. 2002) detect warm temperature ionised gas pervasive to the groups, with densities possibly as high as 10^{-4} cm^{-3} . This clumpy IGM could be associated loosely with galaxies (because of past mergers or disturbances, past bursts etc), or could be simply higher density regions of filaments expected from the cosmic web (Davé et al. 2001). This would also explain the existence of dSphs distant from any large galaxies such as Cetus and Tucana.

We are very grateful to the referee whose comments have greatly improve the paper. This research has made use of NASA’s Astrophysics Data System Bibliographic Services and the NASA/IPAC Extragalactic Database (NED) which is operated by the Jet Propulsion Laboratory, California Institute of Technology, under contract with the National Aeronautics and Space Administration. EDS is grateful for partial support from a NASA LTSARP grant No. NAG5-9221 and the University of Minnesota. BWM is supported by the Gemini Observatory, which is operated by the Association of Universities for Research in Astronomy, Inc., on behalf of the international Gemini partnership of Argentina, Australia, Brazil, Canada, Chile, the United Kingdom, and the United States of America.

A. Appendix: Table of HII regions

The Table 2 below lists all the HII regions positions and luminosities for all the Centaurus A Group dIs.

REFERENCES

- Aguerri, J. A. L., Iglesias-Páramo, J., Vílchez, J. M., Muñoz-Tuñón, C., & Sánchez-Janssen, R. 2005, *AJ*, 130, 475
- Armandroff, T. E., Jacoby, G. H., & Davies, J. E. 1999, *AJ*, 118, 1220
- Babul, A. & Rees, M. J. 1992, *MNRAS*, 255, 346
- Balogh, M., Morris, S., Yee, H., Carlberg, R., Ellingson, E. 1997, *ApJ*, 488, L75
- Banks, G. D., et al. 1999, *ApJ*, 524, 612
- Barkana, R., & Loeb, A. 1999, *ApJ*, 523, 54
- Barnes, D. G. et al. 2001, *MNRAS*, 322, 486
- Beaulieu, S., Freeman, K.C., Carignan, C., & Lockman, F.J. 2006, *AJ*, 131, 325
- Begum, A., & Chengalur, J. N. 2005, *MNRAS*, 362, 609
- Bell, E.F. 2003, *ApJ*, 586, 794
- Binggeli, B., Tarenghi, M., & Sandage, A. 1990, *A&A*, 228, 42
- Blitz, L. & Robishaw, T. 2000, *ApJ*, 541, 675
- Bomans, D.J., Chu, Y.H., & Hopp, U. 1997, *AJ*, 113, 1678
- Bomans, D.J., & Grant, M.-B. 1998, *Astron. Nach.*, 319, 26
- Boissier, S., Gil de Paz, A., Boselli, A. et al. 2007, *ApJ*, 173, 524
- Bouchard, A., Carignan, C., & Mashchenko, S. 2003, *AJ*, 126, 1295
- Bouchard, A., Da Costa, G. S., & Jerjen, H. 2004, *PASP*, 116, 1031
- Bouchard, A., Jerjen, H., Da Costa, G. S., & Ott, J. 2005, *AJ*, 130, 2058
- Bouchard, A., Jerjen, H., Da Costa, G. S., & Ott, J. 2007, *AJ*, 133, 261
- Bouchard, A., Da Costa, G. S., Jerjen, H. 2009, *AJ*, 137, 3038
- Brosch, N., Heller, A., & Almoznino, E. 1998, *MNRAS*, 300, 1091
- Bullock, J.S., Kravtsov, A.V., & Weinberg, D.H. 2000, *ApJ*, 539, 517
- Cannon, J. M., Dohm-Palmer, R. C., Skillman, E. D., Bomans, D. J., Côté, S., & Miller, B. W. 2003, *AJ*, 126, 2806

- Carraro, G., Chiosi, C., Girardi, L., & Lia, C. 2001, *MNRAS*, 327, 69
- Calzetti, D., Conselice, C.J., Gallagher, J.S. & Kinney, A.L. 1999, *AJ*, 118, 797
- Carignan, C., Demers, S. & Côté, S. 1991, *ApJ*, 381, L13
- Chung, A., van Gorkom, J.H., Kenney, J. & Vollmer, B. 2007, *ApJ*, 659, L115
- Conselice, C. J., O’Neil, K., Gallagher, J. S., & Wyse, R. F. G. 2003, *ApJ*, 591, 167
- Conselice, C. J. 2006, *ArXiv Astrophysics e-prints*, arXiv:astro-ph/0605531
- Côté, S. 1995, Ph.D. Thesis, Australian National University
- Côté, S., Carignan, C., & Freeman, K.C. 2000, *AJ*, 120, 3027
- Côté, S., Freeman, K. C., Carignan, C., & Quinn, P. 1997, *AJ*, 114, 1313
- bibitem[Côté et al.(2006)] cpf06 Côté, P., Piatek, S., Ferrarese, L. et al. 2006, *ApJS*, 165, 57
- de Blok, W. J. G., Zwaan, M. A., Dijkstra, M., Briggs, F. H., & Freeman, K. C. 2002, *A&A*, 382, 43
- Da Costa, G. S., Jerjen, H., & Bouchard, A. 2007, *ArXiv Astrophysics e-prints*, arXiv:astro-ph/0710.1420
- Davé, R. et al. 2001, *ApJ*, 552, 473
- Davidge, T.J. 2008, *AJ*, 135, 1636
- De Rijcke, S., Dejonghe, H., Zeilinger, W. W., & Hau, G. K. T. 2004, *A&A*, 426, 53
- de Vaucouleurs, G. 1958, *AJ*, 63, 253
- de Vaucouleurs, G. 1975, in *Stars and Stellar Systems 9, Galaxies and the Universe*, ed. A. Sandage, M. Sandage, & J. Kristian (Chicago: Univ. Chicago Press), 557
- de Vaucouleurs, G. 1979, *AJ*, 84, 1270
- de Vaucouleurs, G., de Vaucouleurs, A., Corwin, H. G. Jr., Buta, R. J., Paturel, G., & Foqué, P. 1991, *Third Reference Catalog of Bright Galaxies*, (New York: Springer) (RC3)
- Dohm-Palmer, R. C. et al. 1997, *AJ*, 114, 2527
- Dohm-Palmer, R. C. et al. 1998, *AJ*, 116, 1227
- Done, C., Madejski, G.M., & Smith, D.A. 1996, *ApJ*, 463, L63
- Efstathiou, G. 1992, *MNRAS*, 256, 43P

- Elmegreen, B. G. 1997, *ApJ*, 477, 196
- Ferguson, A. M. N. 2002, *Ap&SS*, 281, 119
- Ferguson, A. M. N., Wyse, R. F. G., Gallagher, J. S., & Hunter, D. A. 1996, *AJ*, 111, 2265
- Gallagher, J. S., III, & Hunter, D. A. 1987, *AJ*, 94, 43
- Gallagher, J. S., Madsen, G. J., Reynolds, R. J., Grebel, E. K., & Smecker-Hane, T. A. 2003, *ApJ*, 588, 326
- Gallagher, J. S., Tolstoy, E., Dohm-Palmer, R. C., Skillman, E. D., Cole, A., Hoessel, J., Saha, A., & Mateo, M. 1998, *AJ*, 115, 1869
- Gallagher, J. S. in *Starbursts: From 30 Doradus to Lyman Break Galaxies*, eds. R. de Grijs & R. Gonzalez Delgado (Dordrecht: Springer), 11
- Gallart, C., Martinez-Delgado, D., Gomez-Flechoso, M.A., Mateo, M. 2001, *AJ*, 121, 2572
- Gavazzi, G., Catinella, B., Carrasco, L., Boselli, A., & Contursi, A. 1998, *AJ*, 115, 1745
- Gavazzi, G., Boselli, A., Pedotti, P., Gallazzi, A., & Carrasco, L. 2002, *A&A*, 396, 449
- Geha, M., Guhathakurta, P., Rich, R. M., & Cooper, M. C. 2006, *AJ*, 131, 332
- Gnedin, N. 2000, *ApJ*, 535, L75
- Giuricin, G., Marinoni, C., Ceriani, L., & Pisani, A. 2000, *ApJ*, 543, 178
- Grebel, E. K., Gallagher, J. S., III, & Harbeck, D. 2003, *AJ*, 125, 1926
- Grossi, M., Disney, M. J., Pritzl, B. J., Knezek, P. M., Gallagher, J. S., Minchin, R. F., & Freeman, K. C. 2007, *MNRAS*, 374, 107
- Gunn, J. E., & Gott, J. R. I. 1972, *ApJ*, 176, 1
- Heisler, C.A., Hill, T.L., McCall, M.L., Hunstead, R.W. 1997, *MNRAS*, 285, 374
- Hirashita, H. 2000, *PASJ*, 52, 107
- Hodge, P. 1993, in *Star Formation, Galaxies, and the Interstellar Medium*, eds. J. Franco, F. Ferrini, & G. Tenorio-Tagle, Cambridge University Press, 294
- Holtzman, J. A., Smith, G. H., & Grillmair, C. 2000, *AJ*, 120, 3060
- Hoversten, E.A. & Glazebrook, K. 2008, *ApJ*, 675, 163
- Huchtmeier, W. K., Karachentsev, I. D., Karachentseva, V. E., & Ehle, M. 2000, *A&AS*, 141, 469
- Huchtmeier, W. K., Krishna, G., & Petrosian, A. 2005, *A&A*, 434, 887

- Hunter, D. A., Gallagher, J. S., & Rautenkrantz, D. 1982, *ApJS*, 49, 53
- Hunter, D. A., & Gallagher, J. S., III 1986, *PASP*, 98, 5
- Hunter, D. A., Hawley, W. N., & Gallagher, J. S. 1993, *AJ*, 106, 1797
- Hunter, D. A., & Elmegreen, B.G. 2004, *AJ*, 128, 2170
- Iglesias-Páramo, J., & Vílchez, J. M. 1999, *ApJ*, 518, 94
- Irwin, M. & Tolstoy, E. 2002, *MNRAS*, 336, 643
- Irwin, M. et al. 2007, *ApJ*, 656, L13
- Jerjen, H., Freeman, K. C., & Binggeli, B. 1998, *AJ*, 116, 2873
- Jerjen, H. 2000, *AJ*, 119, 166
- Jerjen, H., & Rejkuba, M. 2000, *A&A*, 371, 487
- Kaisin, S., Kasparova, A., Knyazev, A., Karachentsev, I. 2007, *AstL*, 33, 283
- Karachentsev, I. D. 2005, *AJ*, 129, 178
- Karachentsev, I. D., & Kaisin, S. S. 2007, *AJ*, 133, 1883
- Karachentsev, I. D. et al. 2000, *ApJ*, 542, 128
- Karachentsev, I. D., et al. 2002, *A&A*, 385, 21
- Karachentsev, I. D., et al. 2007, *AJ*, 133, 504
- Karachentseva, V.E, & Karachentsev, I.D. 1998, *A&AS*, 127, 409
- Karachentseva, V. E., & Karachentsev, I. D. 2000, *A&AS*, 146, 359
- Kennicutt, R.C. Jr. 1983, *ApJ*, 272, 54
- Kennicutt, R.C. Jr. 1984, *ApJ*, 287, 116
- Kennicutt, R. C., Jr. 1989, *ApJ*, 344, 685
- Kennicutt, R.C. Jr. 1998, *ApJ*, 498, 541
- Kennicutt, R.C. Jr., & Hodge, P.W. 1986, *ApJ*, 306, 130
- Kennicutt, R.C. Jr., & Skillman, E.D. 2001, *AJ*, 121, 1461
- Kennicutt, R.C. Jr., Tamblyn, P., & Congdon, C.W. 1994, *ApJ*, 435, 22
- Kennicutt, R.C. Jr., Lee, J., Funes, J., Sakai, S. & Akiyama, S. 2008, *ApJS*, 178, 247

- Kewley, L. J., Heisler, C. A., Dopita, M. A., & Lumsden, S. 2001, *ApJS*, 132, 37
- Klypin, A., Kravtsov, A. V., Valenzuela, O., & Prada, F. 1999, *ApJ*, 522, 82
- Knezek, P. M., Sembach, K. R., & Gallagher, J. S., III 1999, *ApJ*, 514, 119
- Koopmann, R. & Kenney, J. 2006, *ApJS*, 162, 97
- Larson, R. B., Tinsley, B. M., & Caldwell, C. N. 1980, *ApJ*, 237, 692
- Lauberts, A. 1984, *A&AS*, 58, 249
- Lauberts, A., & Valentijn, E. A. 1989, *The Surface Photometry Catalogue of the ESOUppsala Galaxies*, Garching: European Southern Observatory
- Lee, H., Skillman, E. D., Cannon, J. M., Jackson, D. C., Gehrz, R. D., Polomski, E. F., & Woodward, C. E. 2006, *ApJ*, 647, 970
- Lee, J.C. 2006, PhD Thesis, University of Arizona
- Lee, J.C., Kennicutt, R.C., Funes, J.G., Sakai, S., Akiyama, S. 2009, *ApJ*, 692, 1305
- Lisker, T., Glatt, K., Westera, P., & Grebel, E. K. 2006, *AJ*, 132, 2432
- Lo, K. Y., Sargent, W. L. W., & Young, K. 1993, *AJ*, 106, 507
- Marlowe, A. T., Meurer, G. R., Heckman, T. M., & Schommer, R. 1997, *ApJS*, 112, 285
- Mashchenko, S., Carignan, C., & Bouchard, A. 2004, *MNRAS*, 352, 168
- Mateo, M. 1998, *ARA&A*, 36, 435
- Mayer, L., Governato, F., Colpi, M., Moore, B., Quinn, T., Wadsley, J., Stadel, J., & Lake, G. 2001a, *ApJ*, 547, L123
- Mayer, L., Governato, F., Colpi, M., Moore, B., Quinn, T., Wadsley, J., Stadel, J., & Lake, G. 2001b, *ApJ*, 559, 754
- Mayer, L., Mastropietro, C., Wadsley, J., Stadel, J., & Moore, B. 2006, *MNRAS*, 369, 1021
- Mayer, L., Kazantzidis, S., Mastropietro, C., & Wadsley, J. 2007, *Nature*, 445, 738
- Meurer, G., Hanish, D., Ferguson, H. et al 2006, *ApJS*, 165, 307
- Miller, B. W. 1994, Ph.D. Thesis, University of Washington
- Miller, B. W. 1996, *AJ*, 112, 991
- Miller, B. W., Dolphin, A. E., Lee, M. G., Kim, S. C., & Hodge, P. 2001 *ApJ*, 562, 713

- Miller, B.W., & Hodge, P. 1994, *ApJ*, 427, 656
- Minchin, R. F., et al. 2003, *MNRAS*, 346, 787
- Moore, B., Katz, N., Lake, G., Dressler, A., & Oemler, A. 1996, *Nature*, 379, 613
- Moore, B., Ghigna, S., Governato, F., Lake, G., Quinn, T., Stadel, J., & Tozzi, P. 1999, *ApJ*, 524, L19
- Nicastro, F. et al. 2002, *ApJ*, 573, 157
- Normandeau, M., Taylor, A.R., & Dewdney, P.E. 1996, *Nature*, 380, 687
- Oosterloo, T., Da Costa, G.S., & Staveley-Smith, L. 1996, *AJ*, 112, 1969
- Peebles, P. J. E. 1989, *ApJ*, 344, L53
- Perez-Gonzalez, P., Zamorano, J., Gallego, J. et al. 2003, *ApJ*, 591, 827
- Phillips, M.M., Jenkins, C.R., Dopita, M.A., Sadler, E.M. & Binette, L. 1986, *AJ*, 91, 1062
- Press, W. H., Teukolsky, S. A., Vetterling, W. T., & Flannery, B. P. 1992, *Numerical Recipes in Fortran*, Cambridge University Press
- Prugniel, P., Bica, E., Klotz, A., & Alloin, D. 1993, *A&AS*, 98, 229
- Prugniel, P., & Heraudeau, P. 1998, *A&AS*, 128, 299
- Puche, D., & Carignan, C. 1988, *AJ*, 95, 1025
- Quinn, T., Katz, N., & Efstathiou, G. 1996, *MNRAS*, 278, L49
- Richer, M. G. et al. 2001, *A&A*, 370, 34
- Roberts, M.S. 1963, *ARA&A*, 1, 149
- Rumstay, K. S., & Kaufman, M. 1983, *ApJ*, 274, 611
- Sadler, E. M. 2001, *Gas and Galaxy Evolution*, Eds. J. E. Hibbard, M. Rupen, and J. H. van Gorkom, *ASP Conference Proceedings*, 240, 445
- Sandage, A., & Binggeli, B. 1984, *AJ*, 89, 919
- Sandage, A., & Hoffman, G.L. 1991, *ApJ*, 379, 45
- Scalo, J.M. 1986, *Fund. Cos. Phys.*, 11, 1
- Schaerer, D., Contini, T., & Pindao, M. 1999, *A&AS*, 136, 35
- Schlegel, D.J., Finkbeiner, D.P., & Davis, M. 1998, *ApJ*, 500, 525

- Schaye, J. 2004, *ApJ*, 609, 667
- Sembach, K.R., et al. 2003, *ApJS*, 146, 165
- Skillman, E. D. 1996, *ASP Conf. Ser.* 106: The Minnesota Lectures on Extragalactic Neutral Hydrogen, 208
- Skillman, E. D., Bomans, D. J., & Kobulnicky, H. A. 1997, *ApJ*, 474, 205
- Skillman, E. D., Côté, S., & Miller, B. W. 2003, *AJ*, 125, 593
- Skillman, E. D., Côté, S., & Miller, B. W. 2003, *AJ*, 125, 610
- Skillman, E. D., Terlevich, R., Teuben, P. J., & van Woerden, H. 1988, *A&A*, 198, 33
- St-Germain, J., Carignan, C., Côté, S., & Oosterloo, T. 1999, *AJ*, 118, 1235
- Strobel, N. V., Hodge, P., & Kennicutt, R. C., Jr. 1991, *ApJ*, 383, 148
- Takei, Y., Henry, P., Finoguenov, A. et al. 2007, *ApJ*, 655, 831
- Taylor, C. L., Brinks, E., Pogge, R. W., & Skillman, E. D. 1994, *AJ*, 107, 971
- Thomson, R. C. 1992, *MNRAS*, 257, 689
- Toomre, A. 1964, *ApJ*, 139, 1217
- Tremonti, C.A., Lee, J.C., van Zee, L. et al. 2007, *AAS*, 211, 9503
- Tully, R.B., & Fisher, J.R. 1987, *Nearby Galaxies Atlas*, Cambridge University Press
- van den Bergh, S. 1994a, *AJ*, 107, 1328
- van den Bergh, S. 1994b, *ApJ*, 428, 617
- van den Bergh, S. 2000, *PASP*, 112, 529
- van Zee, L. 2000, *AJ*, 119, 2757
- van Zee, L. 2001, *AJ*, 121, 2003
- van Zee, L., Haynes, M. P., Salzer, J. J., Boriels, A. 1997, *AJ*, 113, 1618
- van Zee, L., Haynes, M. P., & Salzer, J. J. 1997, *AJ*, 114, 2479
- Vorontsov-Vel'Yaminov, B. A., & Ivanišević, G. 1974, *Soviet Astronomy*, 18, 174
- Whiting, A. B. 1999, *AJ*, 117, 202
- Young, L.M., & Lo, K.Y. 1997, *ApJ*, 490, 710

Youngblood, A.J., & Hunter, D.A. 1999, *ApJ*, 519, 55

Table 1. Centaurus A Group Dwarf Irregular Galaxies detected in H α

Galaxy Name	R.A. (J2000)	Dec. (J2000)	V_{\odot}	D (Mpc)	Ref.	M(B)
ESO 381-G20	12:46:00.4	–33:50:17	596	5.45 \pm 0.44	1	–14.89 \pm 0.05
DDO 161	13:03:17.3	–17:25:20	747	3.80		–15.36 \pm 0.07
CEN 6	13:05:01.0	–40:04:04	619	5.78 \pm 0.46	1	–12.94 \pm 0.04
ESO 324-G24	13:27:35.3	–41:28:50	526	3.73 \pm 0.43	2	–14.92 \pm 0.04
UGCA 365	13:36:30.7	–29:14:11	582	5.25 \pm 0.43	1	–13.65 \pm 0.09
ESO 444-G84	13:37:20.1	–28:02:46	591	4.61 \pm 0.46	2	–13.65 \pm 0.04
NGC 5237	13:37:38.9	–42:50:51	369	3.40 \pm 0.27	1	–14.74 \pm 0.04
IC 4316	13:40:18.0	–28:53:40	589	4.41 \pm 0.44	2	–14.03 \pm 0.04
NGC 5264	13:41:36.9	–29:54:50	487	4.53 \pm 0.45	2	–16.03 \pm 0.09
ESO 325-G11	13:45:00.7	–41:51:32	550	3.40 \pm 0.39	2	–13.83 \pm 0.07
ESO 383-G87	13:49:18.7	–36:03:41	333	3.45 \pm 0.27	1	–17.07 \pm 0.09
NGC 5408	14:03:21.4	–41:22:36	506	4.81 \pm 0.48	2	–16.15 \pm 0.05
UKS 1424-460	14:28:03.3	–46:18:13	397	3.58 \pm 0.33	2	–13.54 \pm 0.11
ESO 222-G10	14:35:02.9	–49:25:18	632	3.80		–12.85 \pm 0.04
ESO 272-G25	14:43:25.5	–44:42:19	624	3.80		–13.72 \pm 0.04
ESO 223-G09	15:01:01.3	–48:15:51	593	6.40 \pm 0.51	1	–14.91 \pm 0.06
ESO 274-G01	15:14:11.5	–46:47:39	528	3.05 \pm 0.24	1	–17.25 \pm 0.09

Note. — Heliocentric velocities and magnitudes are from Côté et al. (1997). Distances are from: (1) Karachentsev et al. (2007); (2) Karachentsev et al. (2002).

Table 2. HII Regions Positions and H α Fluxes

Galaxy and Number	R.A. (J2000)	Dec.	H α Flux 10^{-15} ergs cm $^{-2}$ s $^{-1}$	$\log L(H\alpha)$ ergs s $^{-1}$
ESO 381-G020 #1	12:45:53.30	-33:48:48.5	5.2 ± 1.1	37.3
ESO 381-G020 #2	12:45:53.70	-33:48:52.8	8.4 ± 1.2	37.5
ESO 381-G020 #3	12:45:57.40	-33:49:26.3	6.2 ± 0.8	37.3
ESO 381-G020 #4	12:45:58.90	-33:49:58.3	24.0 ± 1.4	37.9
ESO 381-G020 #5	12:45:59.50	-33:50:01.2	5.8 ± 1.1	37.3
ESO 381-G020 #6	12:45:59.00	-33:49:53.0	2.8 ± 0.6	37.0
ESO 381-G020 #7	12:45:59.10	-33:50:34.1	12.2 ± 1.1	37.6
ESO 381-G020 #8	12:45:59.10	-33:50:37.4	9.8 ± 1.0	37.5
ESO 381-G020 #9	12:46:01.50	-33:50:27.9	11.4 ± 1.1	37.6
ESO 381-G020 #10	12:46:01.50	-33:50:24.3	18.8 ± 1.3	37.8
ESO 381-G020 #11	12:46:01.10	-33:50:31.3	2.6 ± 0.5	37.0
ESO 381-G020 #12	12:46:00.90	-33:50:27.6	5.6 ± 0.7	37.3
ESO 381-G020 #13	12:46:01.30	-33:50:34.6	0.7 ± 0.1	36.4
ESO 381-G020 #14	12:46:04.30	-33:50:35.6	4.5 ± 1.1	37.2
ESO 381-G020 #15	12:45:57.60	-33:49:41.2	3.9 ± 1.2	37.1
DDO 161 #1	13:03:02.93	-17:23:35.1	14.7 ± 3.0	37.4
DDO 161 #2	13:03:04.56	-17:24:01.4	1.6 ± 0.5	36.4
DDO 161 #3	13:03:05.89	-17:24:11.3	3.5 ± 0.4	36.8
DDO 161 #4	13:03:06.82	-17:24:08.7	12.7 ± 1.6	37.3
DDO 161 #5	13:03:12.32	-17:24:43.8	6.6 ± 1.7	37.1
DDO 161 #6	13:03:12.62	-17:25:02.0	6.3 ± 1.7	37.0
DDO 161 #7	13:03:14.46	-17:25:04.3	26.3 ± 1.7	37.7
DDO 161 #8	13:03:15.16	-17:25:07.5	82.0 ± 1.7	38.2
DDO 161 #9	13:03:15.50	-17:24:50.9	52.0 ± 1.7	38.0
DDO 161 #10	13:03:14.52	-17:24:52.7	25.1 ± 1.7	37.6
DDO 161 #11	13:03:15.21	-17:24:59.2	5.2 ± 1.7	37.0
DDO 161 #12	13:03:16.13	-17:24:56.7	19.1 ± 1.7	37.5
DDO 161 #13	13:03:16.37	-17:25:02.4	15.3 ± 1.6	37.4
DDO 161 #14	13:03:15.39	-17:25:16.6	5.8 ± 1.1	37.0
DDO 161 #15	13:03:14.51	-17:24:41.9	0.8 ± 0.1	36.1
DDO 161 #16	13:03:14.22	-17:24:45.2	0.8 ± 0.0	36.2

Table 2—Continued

Galaxy and Number	R.A. (J2000)	Dec.	H α Flux 10^{-15} ergs cm $^{-2}$ s $^{-1}$	log $L(H\alpha)$ ergs s $^{-1}$
DDO 161 #17	13:03:13.82	-17:24:52.8	1.4 ± 0.5	36.4
DDO 161 #18	13:03:16.60	-17:25:08.2	17.4 ± 1.6	37.5
DDO 161 #19	13:03:17.06	-17:25:05.7	38.6 ± 1.3	37.8
DDO 161 #20	13:03:17.52	-17:25:06.5	22.9 ± 0.6	37.6
DDO 161 #21	13:03:17.24	-17:25:14.0	110.8 ± 1.7	38.3
DDO 161 #22	13:03:17.76	-17:25:15.6	31.9 ± 1.6	37.7
DDO 161 #23	13:03:17.82	-17:25:23.9	25.2 ± 1.7	37.6
DDO 161 #24	13:03:18.51	-17:25:23.0	34.6 ± 1.7	37.8
DDO 161 #25	13:03:18.92	-17:25:18.8	21.3 ± 1.7	37.6
DDO 161 #26	13:03:18.98	-17:25:25.4	25.8 ± 1.7	37.7
DDO 161 #27	13:03:19.04	-17:25:32.9	4.1 ± 0.5	36.9
DDO 161 #28	13:03:19.85	-17:25:36.9	3.7 ± 0.4	36.8
DDO 161 #29	13:03:20.25	-17:25:37.7	7.4 ± 0.5	37.1
DDO 161 #30	13:03:16.03	-17:25:18.2	10.4 ± 1.7	37.3
DDO 161 #31	13:03:15.98	-17:25:29.9	51.6 ± 1.6	38.0
DDO 161 #32	13:03:15.52	-17:25:33.2	13.8 ± 0.6	37.4
DDO 161 #33	13:03:15.23	-17:25:29.1	2.6 ± 0.5	36.7
DDO 161 #34	13:03:16.04	-17:25:39.8	4.5 ± 1.7	36.9
Centaurus 6 #1	13:05:00.24	-40:04:58.5	6.4 ± 0.8	37.4
Centaurus 6 #2	13:05:00.27	-40:05:02.9	3.6 ± 0.8	37.2
Centaurus 6 #3	13:04:59.99	-40:05:02.0	2.1 ± 0.9	36.9
Centaurus 6 #4	13:04:59.07	-40:05:05.2	1.0 ± 0.7	36.6
ESO 324-G024 #1	13:27:36.00	-41:27:55.0	39.7 ± 1.3	37.8
ESO 324-G024 #2	13:27:36.90	-41:28:12.8	29.6 ± 2.4	37.7
ESO 324-G024 #3	13:27:38.40	-41:29:08.2	5.9 ± 0.3	37.0
ESO 324-G024 #4	13:27:38.70	-41:29:08.2	3.8 ± 0.2	36.8
ESO 324-G024 #5	13:27:38.60	-41:29:57.1	7.9 ± 0.3	37.1
UGCA 365 #1	13:36:32.29	-29:14:18.1	1.2 ± 0.3	36.6

Table 2—Continued

Galaxy and Number	R.A. (J2000)	Dec.	H α Flux 10^{-15} ergs cm $^{-2}$ s $^{-1}$	log $L(H\alpha)$ ergs s $^{-1}$
ESO 444-G84 #1	13:37:16.63	-28:02:20.8	10.1 ± 0.7	37.4
ESO 444-G84 #2	13:37:18.14	-28:02:28.9	8.0 ± 0.5	37.3
ESO 444-G84 #3	13:37:18.03	-28:02:31.2	3.2 ± 0.2	36.9
ESO 444-G84 #4	13:37:18.40	-28:02:55.7	8.2 ± 0.6	37.3
ESO 444-G84 #5	13:37:18.68	-28:02:58.2	11.7 ± 0.7	37.5
NGC 5237 #1	13:37:38.50	-42:50:34.5	237.9 ± 16.4	38.5
NGC 5237 #2	13:37:37.90	-42:50:37.7	80.2 ± 5.0	38.0
NGC 5237 #3	13:37:37.30	-42:50:38.6	18.7 ± 2.8	37.4
NGC 5237 #4	13:37:37.50	-42:50:46.8	18.4 ± 3.0	37.4
NGC 5237 #5	13:37:38.20	-42:50:47.0	41.2 ± 7.0	37.8
NGC 5237 #6	13:37:39.00	-42:50:49.1	24.3 ± 6.0	37.5
IC 4316 #1	13:40:19.04	-28:53:10.4	12.8 ± 0.8	37.5
IC 4316 #2	13:40:18.97	-28:53:15.9	50.2 ± 1.1	38.1
IC 4316 #3	13:40:18.55	-28:53:22.9	18.6 ± 1.1	37.6
IC 4316 #4	13:40:18.50	-28:53:26.0	21.4 ± 1.0	37.7
IC 4316 #5	13:40:19.26	-28:53:23.1	12.8 ± 1.0	37.5
NGC 5264 #1	13:41:39.33	-29:54:18.1	1.4 ± 0.4	36.5
NGC 5264 #2	13:41:38.13	-29:54:32.4	21.6 ± 0.9	37.7
NGC 5264 #3	13:41:37.78	-29:54:35.0	33.7 ± 0.8	37.9
NGC 5264 #4	13:41:33.99	-29:55:15.2	8.6 ± 0.8	37.3
NGC 5264 #5	13:41:33.86	-29:55:08.5	96.6 ± 1.9	38.4
NGC 5264 #6	13:41:33.73	-29:55:02.7	6.7 ± 0.4	37.2
NGC 5264 #7	13:41:36.43	-29:54:57.6	10.2 ± 1.1	37.4
NGC 5264 #8	13:41:37.17	-29:54:57.6	11.1 ± 1.1	37.4
NGC 5264 #9	13:41:37.52	-29:54:56.3	6.2 ± 0.4	37.2
NGC 5264 #10	13:41:37.76	-29:54:52.4	13.8 ± 0.9	37.5
NGC 5264 #11	13:41:38.26	-29:54:54.3	34.5 ± 0.8	37.9
NGC 5264 #12	13:41:38.70	-29:54:48.8	15.1 ± 0.9	37.6
NGC 5264 #13	13:41:38.31	-29:54:45.9	8.6 ± 0.8	37.3

Table 2—Continued

Galaxy and Number	R.A. (J2000)	Dec.	H α Flux 10^{-15} ergs cm $^{-2}$ s $^{-1}$	log $L(H\alpha)$ ergs s $^{-1}$
NGC 5264 #14	13:41:39.02	-29:54:40.4	8.4 ± 0.8	37.3
NGC 5264 #15	13:41:38.72	-29:54:38.8	3.4 ± 0.5	36.9
NGC 5264 #16	13:41:36.69	-29:55:23.4	4.4 ± 0.4	37.0
NGC 5264 #17	13:41:35.48	-29:54:32.0	3.2 ± 0.4	36.9
ESO 325-G011 #1	13:44:56.79	-41:51:02.5	25.4 ± 3.8	37.5
ESO 325-G011 #2	13:44:58.43	-41:51:07.2	75.9 ± 4.9	38.0
ESO 325-G011 #3	13:44:59.71	-41:51:14.2	27.1 ± 3.8	37.6
ESO 325-G011 #4	13:44:58.30	-41:51:26.3	10.4 ± 3.6	37.2
ESO 325-G011 #5	13:45:01.59	-41:52:04.1	34.2 ± 3.8	37.7
ESO 325-G011 #6	13:45:01.67	-41:52:20.0	20.2 ± 1.8	37.4
ESO 325-G011 #7	13:45:06.37	-41:52:21.2	14.2 ± 3.8	37.3
ESO 325-G011 #8	13:45:07.88	-41:52:30.6	18.7 ± 3.7	37.4
ESO 383-G087 #1	13:49:16.49	-36:02:49.3	9.6 ± 1.3	37.1
ESO 383-G087 #2	13:49:15.98	-36:02:58.4	26.4 ± 1.2	37.6
ESO 383-G087 #3	13:49:14.32	-36:03:04.4	3.9 ± 0.6	36.7
ESO 383-G087 #4	13:49:14.39	-36:03:12.6	8.3 ± 0.5	37.1
ESO 383-G087 #5	13:49:15.38	-36:03:17.9	4.3 ± 0.5	36.8
ESO 383-G087 #6	13:49:15.76	-36:03:19.9	11.4 ± 0.5	37.2
ESO 383-G087 #7	13:49:16.17	-36:03:19.5	8.2 ± 1.2	37.1
ESO 383-G087 #8	13:49:18.98	-36:02:54.0	10.2 ± 1.3	37.2
ESO 383-G087 #9	13:49:19.15	-36:03:00.2	9.1 ± 0.5	37.1
ESO 383-G087 #10	13:49:19.50	-36:03:04.3	5.6 ± 0.5	36.9
ESO 383-G087 #11	13:49:18.27	-36:03:11.5	144.3 ± 3.0	38.3
ESO 383-G087 #12	13:49:18.58	-36:03:04.8	13.1 ± 1.3	37.3
ESO 383-G087 #13	13:49:19.03	-36:03:15.5	18.0 ± 1.5	37.4
ESO 383-G087 #14	13:49:18.21	-36:03:21.8	20.0 ± 1.7	37.5
ESO 383-G087 #15	13:49:17.29	-36:03:13.6	28.0 ± 3.6	37.6
ESO 383-G087 #16	13:49:18.66	-36:03:27.6	17.3 ± 1.9	37.4
ESO 383-G087 #17	13:49:17.74	-36:03:37.1	68.9 ± 2.4	38.0
ESO 383-G087 #18	13:49:14.17	-36:03:42.8	20.0 ± 1.8	37.5

Table 2—Continued

Galaxy and Number	R.A. (J2000)	Dec.	H α Flux 10^{-15} ergs cm $^{-2}$ s $^{-1}$	log $L(H\alpha)$ ergs s $^{-1}$
ESO 383-G087 #19	13:49:14.35	-36:04:03.0	9.7 ± 1.4	37.1
ESO 383-G087 #20	13:49:14.36	-36:04:13.8	15.5 ± 2.1	37.4
ESO 383-G087 #21	13:49:15.55	-36:04:08.3	37.9 ± 1.3	37.7
ESO 383-G087 #22	13:49:16.02	-36:04:02.1	99.5 ± 2.4	38.2
ESO 383-G087 #23	13:49:15.13	-36:03:59.7	20.1 ± 1.9	37.5
ESO 383-G087 #24	13:49:16.25	-36:03:53.4	19.1 ± 1.5	37.4
ESO 383-G087 #25	13:49:19.98	-36:04:07.5	14.8 ± 1.9	37.3
ESO 383-G087 #26	13:49:22.20	-36:03:16.1	13.4 ± 1.5	37.3
ESO 383-G087 #27	13:49:21.51	-36:03:01.3	13.7 ± 1.7	37.3
ESO 383-G087 #28	13:49:24.46	-36:02:51.9	8.3 ± 0.5	37.1
ESO 383-G087 #29	15:14:07.70	-46:49:49.7	9.2 ± 0.5	37.1
NGC 5408 #1	14:03:28.00	-41:21:54.6	4.0 ± 0.2	37.0
NGC 5408 #2	14:03:27.53	-41:21:52.7	5.3 ± 0.2	37.2
NGC 5408 #3	14:03:26.70	-41:22:04.1	30.4 ± 0.7	37.9
NGC 5408 #4	14:03:26.84	-41:22:21.8	9.6 ± 0.4	37.4
NGC 5408 #5	14:03:26.45	-41:22:29.3	24.6 ± 2.4	37.8
NGC 5408 #6	14:03:25.69	-41:22:32.1	2.6 ± 0.2	36.9
NGC 5408 #7	14:03:26.01	-41:22:34.1	9.2 ± 0.4	37.4
NGC 5408 #8	14:03:26.31	-41:22:39.8	49.4 ± 0.4	38.1
NGC 5408 #9	14:03:25.94	-41:22:40.1	13.3 ± 0.4	37.6
NGC 5408 #10	14:03:27.24	-41:22:48.0	5.5 ± 0.2	37.2
NGC 5408 #11	14:03:25.11	-41:21:55.4	16.0 ± 1.6	37.6
NGC 5408 #12	14:03:24.05	-41:21:55.8	21.5 ± 0.6	37.8
NGC 5408 #13	14:03:23.66	-41:21:53.6	4.3 ± 0.2	37.1
NGC 5408 #14	14:03:23.46	-41:21:52.8	5.7 ± 0.2	37.2
NGC 5408 #15	14:03:23.10	-41:21:55.3	4.2 ± 0.2	37.1
NGC 5408 #16	14:03:22.81	-41:22:03.1	61.5 ± 1.3	38.2
NGC 5408 #17	14:03:22.29	-41:22:03.4	12.8 ± 0.2	37.6
NGC 5408 #18	14:03:23.70	-41:22:25.7	13.6 ± 0.6	37.6
NGC 5408 #19	14:03:23.21	-41:22:30.7	7.2 ± 0.4	37.3
NGC 5408 #20	14:03:23.31	-41:22:34.0	4.5 ± 0.2	37.1

Table 2—Continued

Galaxy and Number	R.A. (J2000)	Dec.	H α Flux 10^{-15} ergs cm $^{-2}$ s $^{-1}$	log $L(H\alpha)$ ergs s $^{-1}$
NGC 5408 #21	14:03:24.22	-41:22:35.3	2.3 ± 0.1	36.8
NGC 5408 #22	14:03:23.95	-41:22:38.1	3.3 ± 0.1	37.0
NGC 5408 #23	14:03:23.96	-41:22:44.5	5.0 ± 0.3	37.1
NGC 5408 #24	14:03:23.56	-41:22:39.0	36.7 ± 0.3	38.0
NGC 5408 #25	14:03:23.02	-41:22:38.7	21.5 ± 0.4	37.8
NGC 5408 #26	14:03:23.32	-41:22:41.8	7.6 ± 0.1	37.3
NGC 5408 #27	14:03:23.42	-41:22:47.8	17.9 ± 0.7	37.7
NGC 5408 #28	14:03:22.68	-41:22:35.4	8.3 ± 0.2	37.4
NGC 5408 #29	14:03:22.51	-41:22:38.5	26.0 ± 0.2	37.9
NGC 5408 #30	14:03:22.83	-41:22:44.6	6.7 ± 0.2	37.3
NGC 5408 #31	14:03:22.49	-41:22:49.3	14.6 ± 0.3	37.6
NGC 5408 #32	14:03:22.24	-41:22:44.9	18.5 ± 0.2	37.7
NGC 5408 #33	14:03:21.77	-41:22:43.5	5.5 ± 0.2	37.2
NGC 5408 #34	14:03:21.48	-41:22:44.9	2.7 ± 0.2	36.9
NGC 5408 #35	14:03:22.75	-41:22:32.4	3.9 ± 0.1	37.0
NGC 5408 #36	14:03:21.51	-41:22:50.5	17.4 ± 0.4	37.7
NGC 5408 #37	14:03:21.06	-41:22:36.1	59.6 ± 0.9	38.2
NGC 5408 #38	14:03:20.64	-41:22:40.9	47.2 ± 0.4	38.1
NGC 5408 #39	14:03:20.89	-41:22:45.3	19.2 ± 0.3	37.7
NGC 5408 #40	14:03:21.06	-41:22:50.0	42.5 ± 0.5	38.1
NGC 5408 #41	14:03:20.30	-41:22:46.2	20.0 ± 0.4	37.7
NGC 5408 #42	14:03:21.13	-41:22:42.2	12.1 ± 0.3	37.5
NGC 5408 #43	14:03:19.78	-41:22:28.0	37.6 ± 0.7	38.0
NGC 5408 #44	14:03:20.25	-41:22:38.7	8.0 ± 0.2	37.3
NGC 5408 #45	14:03:19.93	-41:22:40.9	30.2 ± 0.3	37.9
NGC 5408 #46	14:03:19.30	-41:22:46.0	483.5 ± 1.1	39.1
NGC 5408 #47	14:03:18.59	-41:22:52.1	1874.1 ± 12.1	39.7
NGC 5408 #48	14:03:19.32	-41:22:50.9	401.0 ± 0.8	39.0
NGC 5408 #49	14:03:19.86	-41:22:46.7	53.1 ± 0.3	38.2
NGC 5408 #50	14:03:17.98	-41:22:54.1	48.8 ± 0.4	38.1
NGC 5408 #51	14:03:19.52	-41:22:59.8	40.2 ± 0.3	38.0
NGC 5408 #52	14:03:17.61	-41:22:53.6	27.0 ± 0.2	37.9

Table 2—Continued

Galaxy and Number	R.A. (J2000)	Dec.	H α Flux 10^{-15} ergs cm $^{-2}$ s $^{-1}$	log $L(H\alpha)$ ergs s $^{-1}$
NGC 5408 #53	14:03:17.91	-41:22:58.0	24.8 \pm 0.4	37.8
NGC 5408 #54	14:03:18.10	-41:23:02.1	40.8 \pm 0.4	38.1
NGC 5408 #55	14:03:17.49	-41:23:01.6	20.4 \pm 0.3	37.8
NGC 5408 #56	14:03:17.76	-41:23:07.7	15.5 \pm 0.3	37.6
NGC 5408 #57	14:03:17.34	-41:22:46.7	16.1 \pm 0.4	37.7
NGC 5408 #58	14:03:20.16	-41:22:52.5	3.9 \pm 0.2	37.0
NGC 5408 #59	14:03:20.09	-41:22:57.2	31.3 \pm 0.3	37.9
NGC 5408 #60	14:03:20.72	-41:22:56.3	26.6 \pm 0.3	37.9
NGC 5408 #61	14:03:18.15	-41:23:35.5	22.5 \pm 0.6	37.8
NGC 5408 #62	14:03:18.53	-41:22:38.8	3.0 \pm 0.2	36.9
NGC 5408 #63	14:03:17.61	-41:22:37.8	5.6 \pm 0.1	37.2
UKS 1424-460 #1	14:28:02.00	-46:17:57.0	11.9 \pm 1.0	37.3
ESO 222-G010 #1	14:35:01.80	-49:25:21.7	13.6 \pm 1.1	37.4
ESO 222-G010 #2	14:35:02.20	-49:25:24.8	10.0 \pm 0.9	37.2
ESO 222-G010 #3	14:35:02.76	-49:25:24.4	11.3 \pm 1.0	37.3
ESO 222-G010 #4	14:35:02.58	-49:25:28.4	46.6 \pm 0.5	37.9
ESO 222-G010 #5	14:35:02.73	-49:25:15.6	47.7 \pm 2.5	37.9
ESO 272-G025 #1	14:43:24.10	-44:42:25.4	8.3 \pm 1.2	37.2
ESO 272-G025 #2	14:43:24.45	-44:42:26.1	9.3 \pm 1.5	37.2
ESO 272-G025 #3	14:43:24.30	-44:42:19.9	4.8 \pm 1.0	36.9
ESO 272-G025 #4	14:43:25.08	-44:42:24.1	15.4 \pm 3.2	37.4
ESO 272-G025 #5	14:43:24.98	-44:42:16.1	21.9 \pm 1.6	37.6
ESO 272-G025 #6	14:43:26.29	-44:42:09.4	17.9 \pm 1.7	37.5
ESO 272-G025 #7	14:43:25.96	-44:42:12.0	3.6 \pm 0.7	36.8
ESO 272-G025 #8	14:43:26.34	-44:42:13.9	2.6 \pm 0.5	36.7
ESO 272-G025 #9	14:43:26.42	-44:42:02.7	19.2 \pm 2.5	37.5
ESO 272-G025 #10	14:43:24.53	-44:42:14.1	2.6 \pm 0.7	36.7
ESO 223-G009 #1	15:01:17.54	-48:16:40.0	19.3 \pm 5.2	38.0

Table 2—Continued

Galaxy and Number	R.A. (J2000)	Dec.	H α Flux 10^{-15} ergs cm $^{-2}$ s $^{-1}$	log $L(H\alpha)$ ergs s $^{-1}$
ESO 223-G009 #2	15:01:16.88	-48:16:39.6	7.6 \pm 1.0	37.6
ESO 223-G009 #3	15:01:14.83	-48:19:39.5	69.4 \pm 3.3	38.5
ESO 223-G009 #4	15:01:16.45	-48:19:34.3	6.4 \pm 1.1	37.5
ESO 223-G009 #5	15:01:16.08	-48:19:31.4	18.1 \pm 0.7	38.0
ESO 223-G009 #6	15:01:16.70	-48:19:26.6	2.7 \pm 1.2	37.1
ESO 223-G009 #7	15:01:15.89	-48:19:23.3	6.3 \pm 1.4	37.5
ESO 223-G009 #8	15:01:11.76	-48:18:13.7	7.7 \pm 1.0	37.6
ESO 223-G009 #9	15:01:04.33	-48:17:55.1	199.3 \pm 1.2	39.0
ESO 223-G009 #10	15:01:04.66	-48:17:50.0	55.5 \pm 0.7	38.4
ESO 223-G009 #11	15:01:03.12	-48:17:49.7	9.6 \pm 1.5	37.7
ESO 223-G009 #12	15:01:04.91	-48:17:44.4	20.9 \pm 1.4	38.0
ESO 223-G009 #13	15:01:05.91	-48:17:55.8	36.3 \pm 0.7	38.3
ESO 223-G009 #14	15:01:05.36	-48:17:50.7	40.1 \pm 0.7	38.3
ESO 223-G009 #15	15:01:15.88	-48:17:26.8	20.6 \pm 1.5	38.0
ESO 223-G009 #16	15:01:18.06	-48:18:33.8	5.6 \pm 1.4	37.4
ESO 223-G009 #17	15:01:09.81	-48:17:58.0	19.0 \pm 0.7	38.0
ESO 223-G009 #18	15:01:11.42	-48:17:49.1	22.0 \pm 0.6	38.0
ESO 223-G009 #19	15:01:10.75	-48:17:48.3	18.6 \pm 0.7	38.0
ESO 223-G009 #20	15:01:10.09	-48:17:46.2	9.7 \pm 1.4	37.7
ESO 223-G009 #21	15:01:09.65	-48:17:44.7	6.1 \pm 1.4	37.5
ESO 223-G009 #22	15:01:07.44	-48:17:33.0	15.8 \pm 0.7	37.9
ESO 223-G009 #23	15:01:07.14	-48:17:19.7	13.5 \pm 0.7	37.8
ESO 223-G009 #24	15:01:07.13	-48:17:4.2	13.0 \pm 1.1	37.8
ESO 223-G009 #25	15:01:04.99	-48:16:46.6	9.1 \pm 0.9	37.7
ESO 223-G009 #26	15:01:02.80	-48:17:6.5	53.8 \pm 0.6	38.4
ESO 223-G009 #27	15:01:02.35	-48:16:59.9	23.8 \pm 0.6	38.1
ESO 223-G009 #28	15:01:02.57	-48:16:51.1	26.9 \pm 0.5	38.1
ESO 223-G009 #29	15:01:03.37	-48:16:45.2	11.7 \pm 0.9	37.8
ESO 223-G009 #30	15:01:03.14	-48:16:34.1	19.1 \pm 2.5	38.0
ESO 223-G009 #31	15:01:06.05	-48:15:47.6	10.5 \pm 1.6	37.7
ESO 223-G009 #32	15:01:05.30	-48:17:9.4	3.3 \pm 1.3	37.2
ESO 223-G009 #33	15:01:04.85	-48:17:4.3	5.0 \pm 1.3	37.4

Table 2—Continued

Galaxy and Number	R.A. (J2000)	Dec.	H α Flux 10^{-15} ergs cm $^{-2}$ s $^{-1}$	log $L(H\alpha)$ ergs s $^{-1}$
ESO 223-G009 #34	15:01:03.75	-48:16:59.9	13.3 \pm 0.8	37.8
ESO 223-G009 #35	15:01:07.52	-48:17:45.5	27.4 \pm 0.5	38.1
ESO 223-G009 #36	15:01:10.28	-48:18:44.4	14.4 \pm 0.7	37.9
ESO 223-G009 #37	15:01:09.43	-48:17:41.0	10.7 \pm 1.5	37.7
ESO 223-G009 #38	15:01:03.56	-48:17:49.3	10.3 \pm 1.5	37.7
ESO 223-G009 #39	15:01:04.96	-48:17:59.6	9.1 \pm 1.4	37.7
ESO 223-G009 #40	15:01:03.46	-48:17:10.2	6.9 \pm 1.4	37.5
ESO 274-G001 #1	15:14:30.40	-46:44:40.7	100.0 \pm 4.4	38.0
ESO 274-G001 #2	15:14:28.80	-46:44:56.1	39.6 \pm 2.9	37.6
ESO 274-G001 #3	15:14:29.20	-46:45:08.2	7.6 \pm 0.7	36.9
ESO 274-G001 #4	15:14:28.40	-46:45:09.9	10.6 \pm 1.3	37.1
ESO 274-G001 #5	15:14:17.60	-46:47:16.6	20.3 \pm 1.3	37.4
ESO 274-G001 #6	15:14:17.70	-46:47:23.8	27.2 \pm 1.2	37.5
ESO 274-G001 #7	15:14:16.60	-46:47:36.8	15.9 \pm 1.3	37.3
ESO 274-G001 #8	15:14:15.60	-46:47:57.0	35.2 \pm 3.4	37.6
ESO 274-G001 #9	15:14:14.60	-46:48:17.3	148.0 \pm 1.9	38.2
ESO 274-G001 #10	15:14:14.80	-46:48:09.2	46.0 \pm 1.5	37.7
ESO 274-G001 #11	15:14:13.70	-46:48:12.5	89.7 \pm 1.1	38.0
ESO 274-G001 #12	15:14:13.20	-46:48:19.8	31.1 \pm 1.3	37.5
ESO 274-G001 #13	15:14:14.00	-46:48:23.0	32.3 \pm 0.8	37.6
ESO 274-G001 #14	15:14:13.80	-46:48:35.9	27.1 \pm 2.2	37.5
ESO 274-G001 #15	15:14:13.00	-46:48:30.3	15.8 \pm 1.1	37.2
ESO 274-G001 #16	15:14:13.00	-46:49:02.6	28.7 \pm 2.6	37.5
ESO 274-G001 #17	15:14:12.70	-46:48:58.6	14.7 \pm 0.5	37.2
ESO 274-G001 #18	15:14:12.00	-46:48:56.2	23.5 \pm 0.7	37.4
ESO 274-G001 #19	15:14:11.10	-46:48:53.8	39.5 \pm 1.1	37.6
ESO 274-G001 #20	15:14:11.00	-46:49:05.9	32.9 \pm 1.2	37.6
ESO 274-G001 #21	15:14:12.00	-46:49:03.5	37.4 \pm 1.2	37.6
ESO 274-G001 #22	15:14:12.70	-46:49:10.7	52.5 \pm 1.3	37.8
ESO 274-G001 #23	15:14:10.00	-46:49:02.0	446.2 \pm 3.4	38.7
ESO 274-G001 #24	15:14:10.50	-46:49:22.9	9.5 \pm 0.6	37.0

Table 2—Continued

Galaxy and Number	R.A. (J2000)	Dec.	H α Flux 10^{-15} ergs cm $^{-2}$ s $^{-1}$	$\log L(H\alpha)$ ergs s $^{-1}$
ESO 274-G001 #25	15:14:09.80	-46:49:19.7	9.8 ± 0.6	37.0
ESO 274-G001 #26	15:14:09.30	-46:49:17.3	11.3 ± 0.5	37.1
ESO 274-G001 #27	15:14:08.80	-46:49:20.6	28.6 ± 1.6	37.5
ESO 274-G001 #28	15:14:08.30	-46:49:56.1	30.7 ± 1.1	37.5
ESO 274-G001 #29	15:14:07.70	-46:49:49.7	26.2 ± 1.3	37.5
ESO 274-G001 #30	15:14:05.20	-46:50:12.5	54.9 ± 1.5	37.8
ESO 274-G001 #31	15:14:05.20	-46:50:18.9	27.9 ± 0.6	37.5
ESO 274-G001 #32	15:14:05.20	-46:50:26.2	16.2 ± 0.7	37.3
ESO 274-G001 #33	15:13:58.90	-46:51:46.5	28.1 ± 2.4	37.5
ESO 274-G001 #34	15:14:14.00	-46:48:00.4	37.9 ± 3.5	37.6

Table 3. Star Formation Properties of Centaurus A Group dI Galaxies

Galaxy	SFR $M_{\odot} \text{ yr}^{-1}$	SFR/L(B) $M_{\odot} \text{ yr}^{-1} L_{\odot}^{-1}$	τ_{form} Gyr	M(HI) ^a $10^6 M_{\odot}$	M(HI)/L(B) M_{\odot}/L_{\odot}	τ_{gas} ^b Gyr	SFR/area $M_{\odot} \text{ yr}^{-1} \text{ pc}^{-2}$
ESO 321-G14 ^c	6.5×10^{-4}	4.9×10^{-11}	20	15	1.13	25	
ESO 381-G20	3.4×10^{-3}	2.5×10^{-11}	41	224	1.59	85	-9.30
UGCA 319 ^c	1.4×10^{-4}	5.9×10^{-12}	158	24.0	1.04	200	
DDO 161	1.0×10^{-2}	4.8×10^{-11}	21	375	1.73	48	-8.45
CEN 6	4.2×10^{-4}	1.8×10^{-11}	56	34.7	1.48	110	-9.72
ESO 269-G58 ^d	2.4×10^{-4}	7.9×10^{-13}	1267	24.8	0.08	136.4	
AM1321-304 ^c	4.5×10^{-5}	6.2×10^{-12}	158	20.0	2.74	398	
ESO 324-G24	1.9×10^{-3}	1.3×10^{-11}	77	171	1.18	120	-9.46
UGCA 365	3.2×10^{-5}	7.0×10^{-13}	1422	29.8	0.67	1250	-10.83
ESO 444-G84	8.3×10^{-4}	1.9×10^{-11}	54	98.1	2.18	155	-9.22
NGC 5237	4.6×10^{-3}	3.8×10^{-11}	27	20.7	0.17	5.9	-7.90
IC 4316	2.1×10^{-3}	3.4×10^{-11}	30	35.7	0.56	22	-8.77
NGC 5264	5.9×10^{-3}	1.5×10^{-11}	68	66.2	0.16	14.8	-8.70
ESO 325-G11	2.5×10^{-3}	4.7×10^{-11}	21.4	69.2	1.30	37	-9.70
ESO 383-G87	8.4×10^{-3}	7.9×10^{-12}	126	71.2	0.07	11.3	-8.54
ESO 384-G16 ^e	2.2×10^{-4}	6.6×10^{-12}	152	6.5	0.19	39	
NGC 5408	8.8×10^{-2}	2.0×10^{-10}	5.1	357	0.80	5.3	-7.35
UKS 1424-460	1.4×10^{-4}	3.6×10^{-12}	281	58.4	1.44	534	-11.45
ESO 222-G10	1.8×10^{-3}	8.3×10^{-11}	12.1	31.0	1.44	23	-9.14
ESO 272-G25	1.5×10^{-3}	3.0×10^{-11}	33	<6.5	<0.14	<5.9	-8.48
ESO 223-G09	3.4×10^{-2}	8.6×10^{-11}	11.6	928	2.28	35	-8.28
ESO 274-G01	1.5×10^{-2}	1.2×10^{-11}	82	256	0.21	22	-8.95

^aTotal galaxy HI mass from Côté et al. (1997), adjusted to the distance in Table 1

^b τ_{gas} is the gas depletion time scale = (Total Gas Mass)/(SFR), where the total gas mass is $1.32 \times M(\text{HI})$ to account for He

^cFrom Bouchard et al 2009

^dH α data from Phillips et al. (1986), HI mass from Banks et al. (1999), using the nominal distance of 3.8 Mpc.

^eH α data from Bouchard et al. (2009), HI mass from Beaulieu et al. (2006), using a distance of 4.23 Mpc from Jerjen (2000)

Fig. 1.— Images of 17 Centaurus A Group dwarf irregular galaxies. The r-band images of the galaxies are shown in the left panels and the continuum subtracted $H\alpha$ images are shown in the right panels. The HII regions are labeled and their fluxes are listed in Table 2. The field of view is $150'' \times 150''$, except for Cen6, NGC 5237, IC 4316, ESO 222-G10, ESO 272-G25 ($75'' \times 75''$), ESO 325-G11, ESO 383-G87, ESO 223-G09 ($300'' \times 300''$), DDO 161 ($330'' \times 330''$), and ESO 274-G01 ($540'' \times 540''$). SEE BETTER FIGS IN AJ PAPER

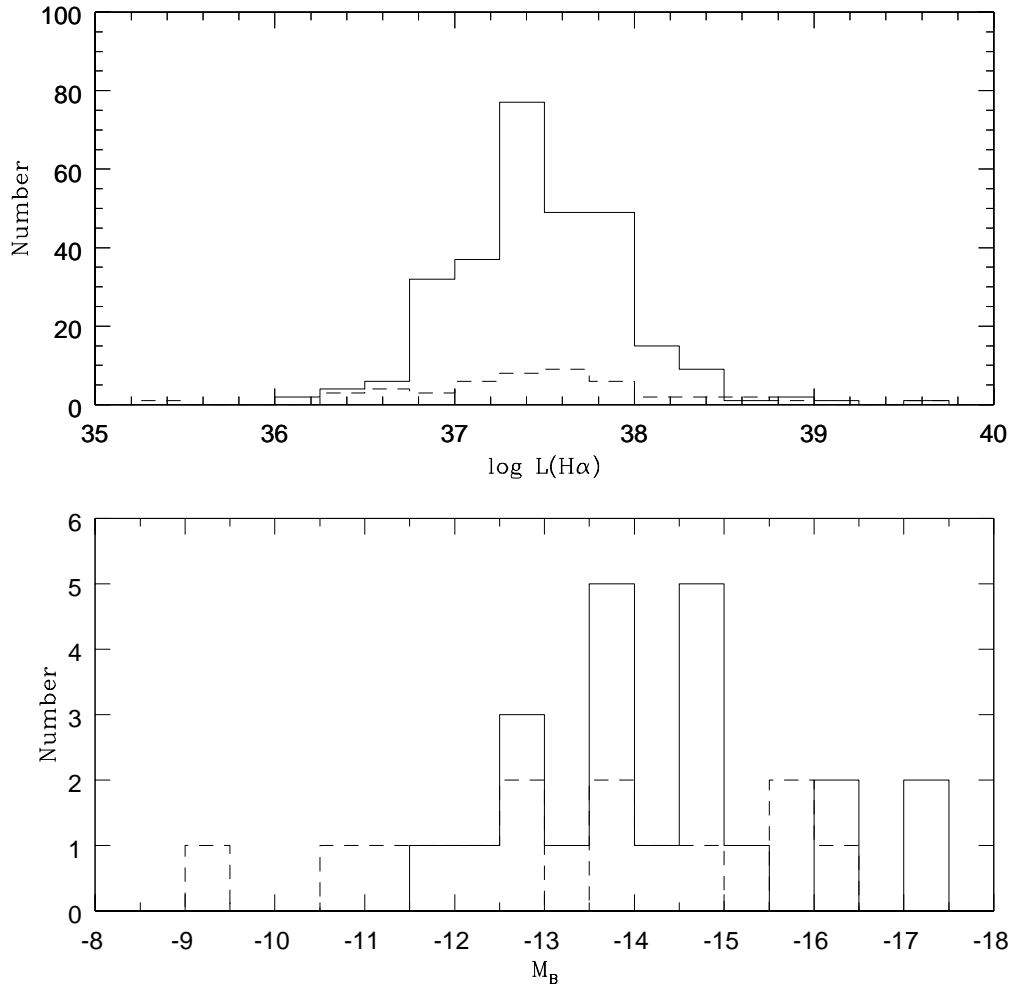


Fig. 2.— Top: histogram of the HII region luminosities for the Centaurus A Group dIIs. The dashed line histogram is for the Sculptor Group dIIs (Skillman et al. 2003a). Bottom: histogram of absolute B magnitudes for the Centaurus A Group and Sculptor Group dIIs. The full line is for the Centaurus A Group, and dash for the Sculptor Group.

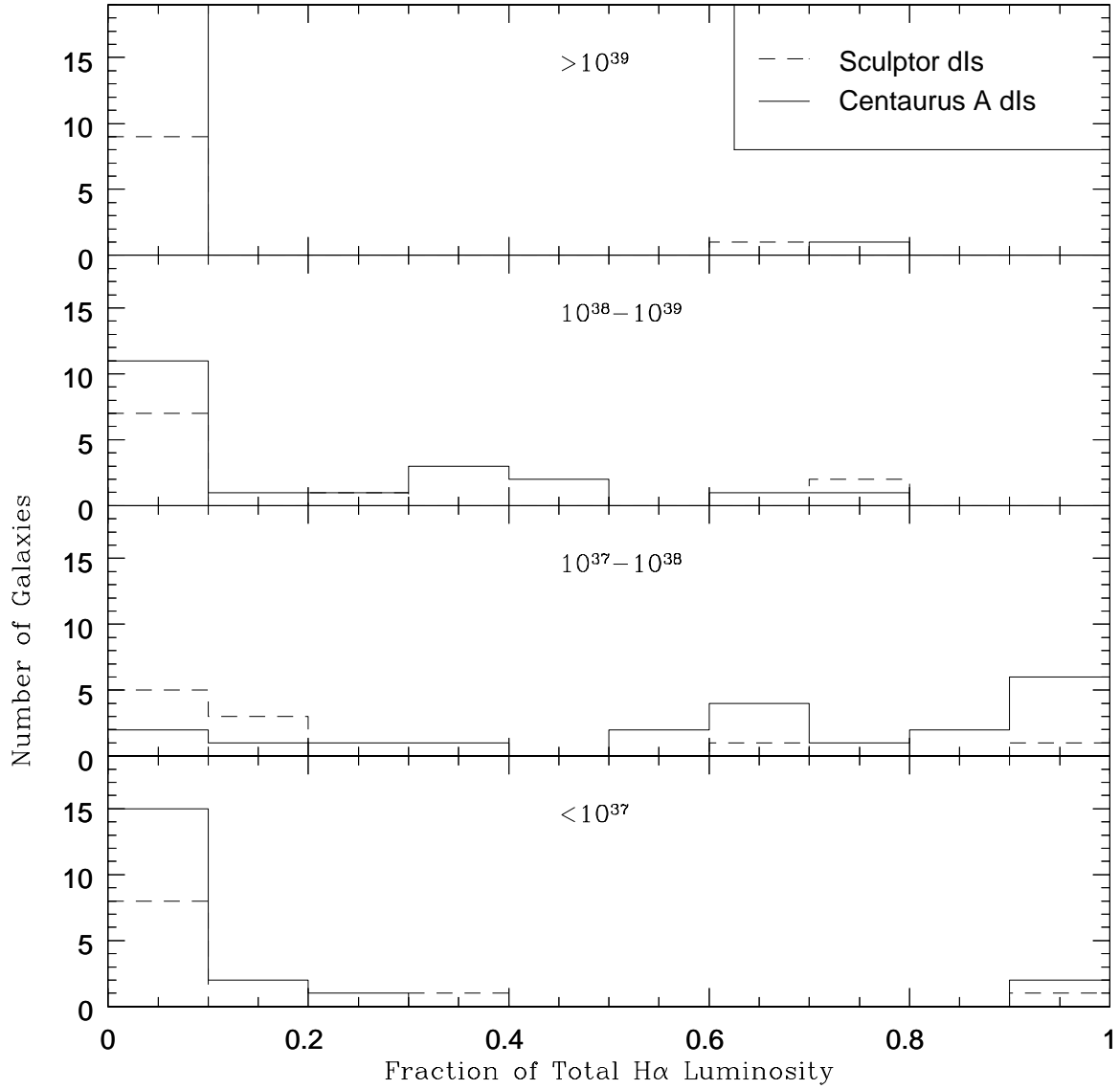


Fig. 3.— Fraction of the total H α luminosity in each galaxy that is contributed by HII regions of a particular luminosity range, ranging from regions with luminosities like that of the Orion nebula $\sim 10^{37}$ erg s $^{-1}$ (bottom) to supergiant HII regions with $L \geq 10^{39}$ erg s $^{-1}$ (top).

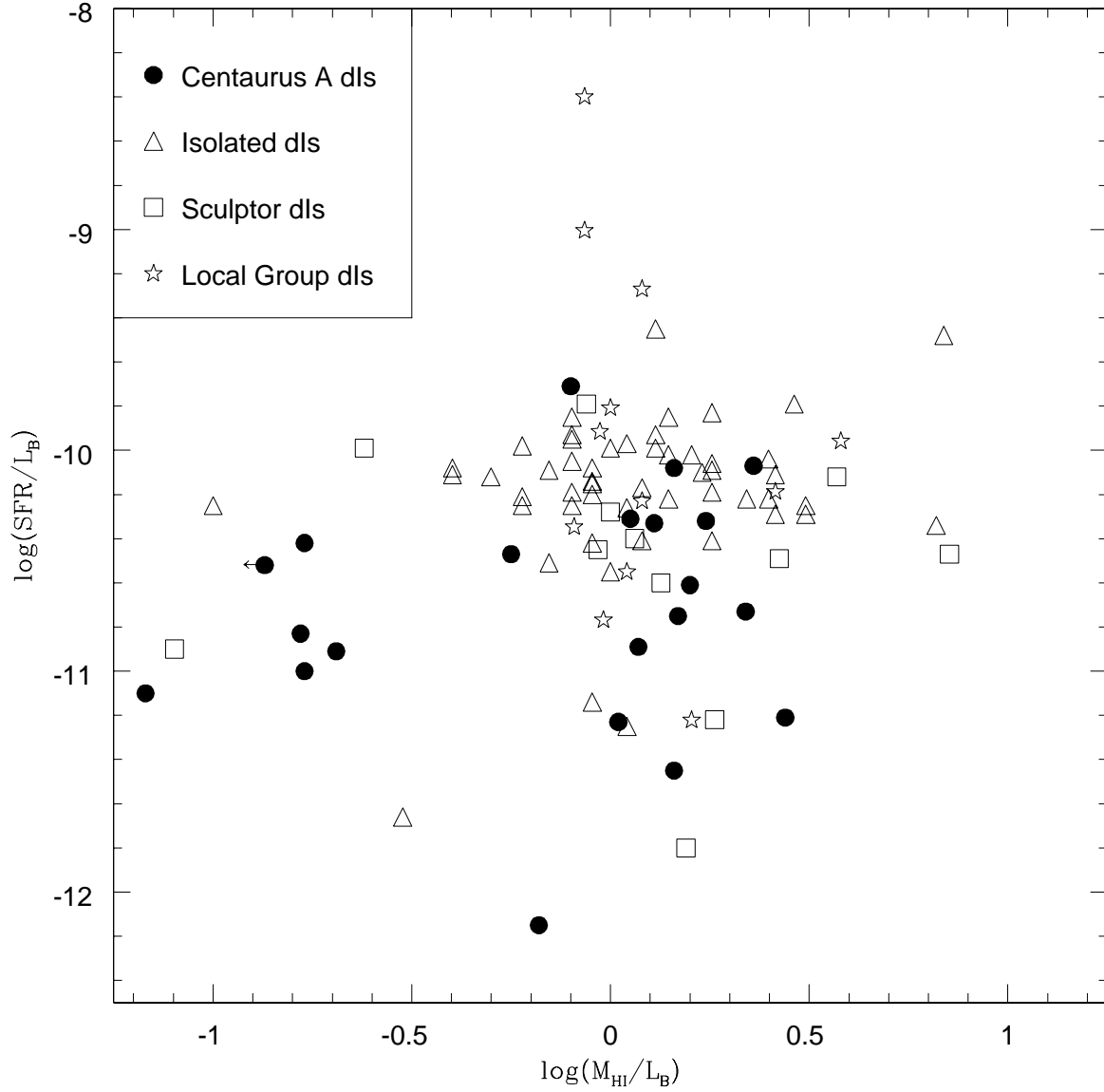


Fig. 4.— A comparison of SFR and gas mass normalized to the galaxy luminosity for the Centaurus A Group dIs and three comparison groups: the Local Group dIs (from Mateo 1998), the Sculptor Group dIs (from Skillman *et al.* 2003), and the isolated dIs of van Zee (2001).

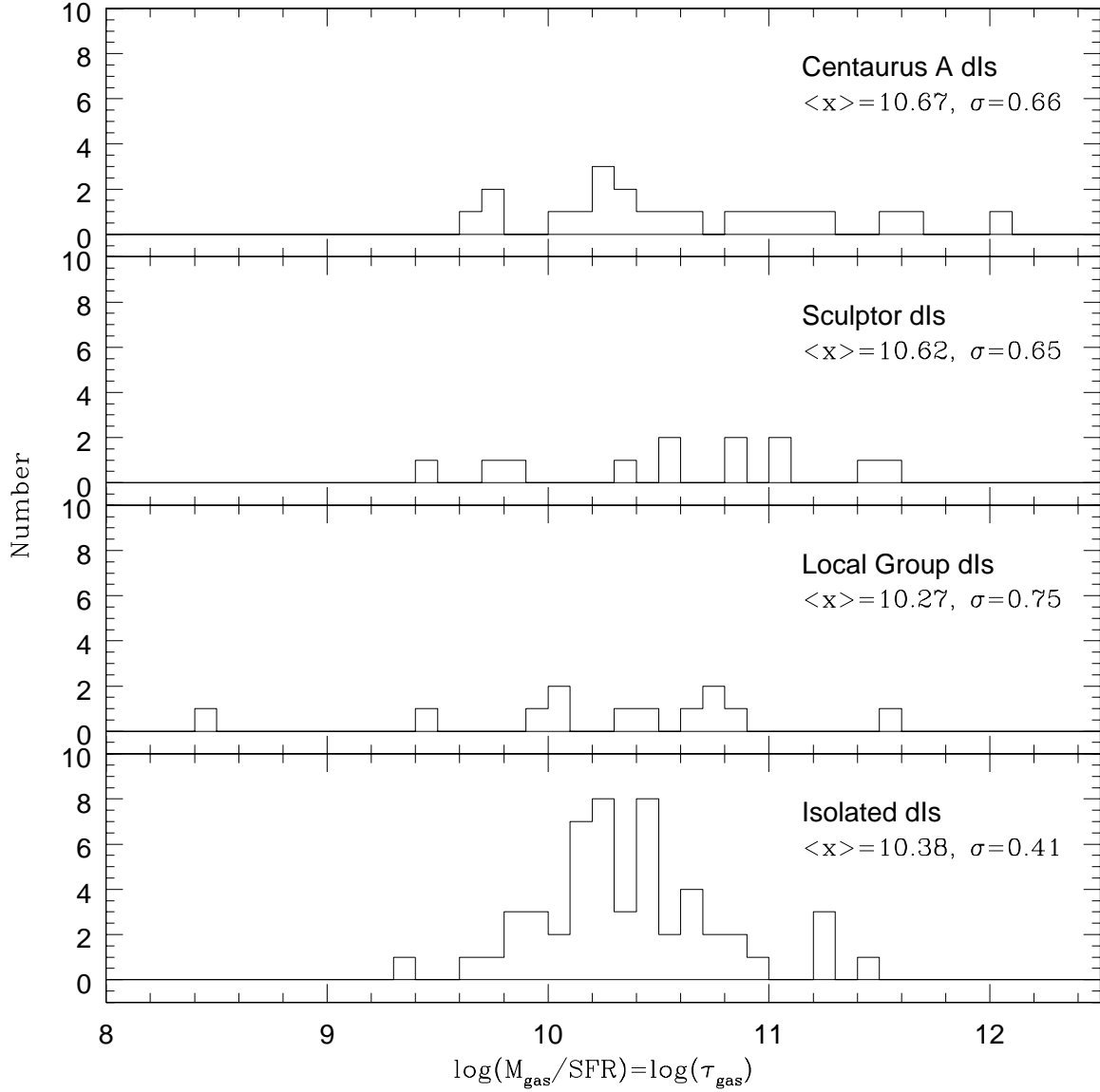


Fig. 5.— A comparison of the ratio of the gas mass to the current star formation rate ($= \tau_{\text{gas}}$) for the Centaurus A Group dIs and three comparison groups: the Sculptor Group dIs (Skillman *et al.* 2003), the Local Group dIs (from Mateo 1998), and the isolated dIs of van Zee (2001). For each sample, the mean value and the standard deviation in the sample is given.

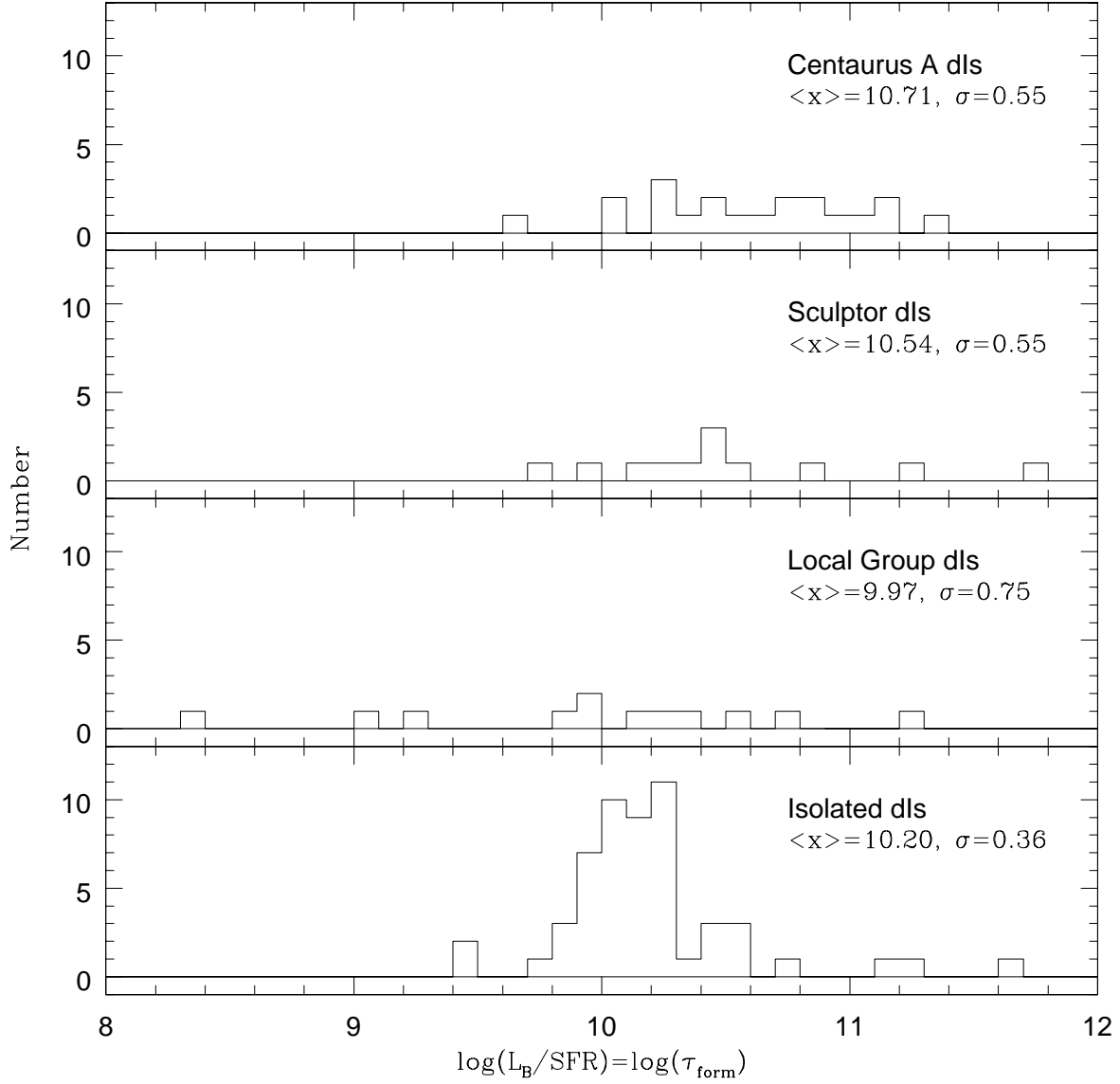


Fig. 6.— A comparison of the ratio of the luminosity to the current star formation rate ($= \tau_{form}$) for the Centaurus A Group dIs and three comparison groups: the Sculptor Group dIs (Skillman *et al.* 2003), the Local Group dIs (from Mateo 1998), and the isolated dIs of van Zee (2001). For each sample, the mean value and the standard deviation in the sample is given.

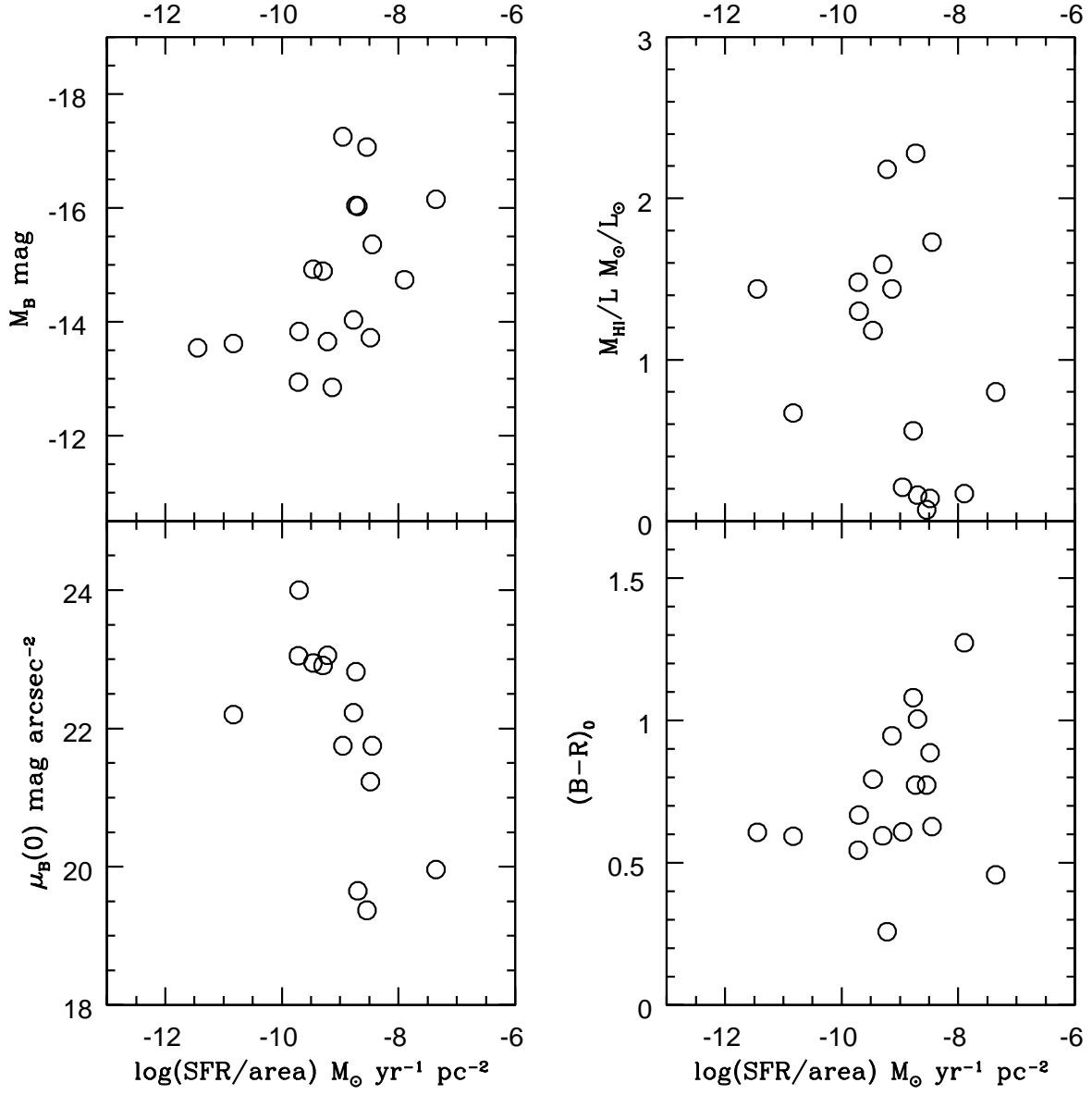


Fig. 7.— The star formation rates per unit area plotted against various global parameters: the absolute B magnitude M_B ; the B central surface brightness μ_0 ; the HI mass to luminosity ratio M_{HI}/L_B ; the color B-R.

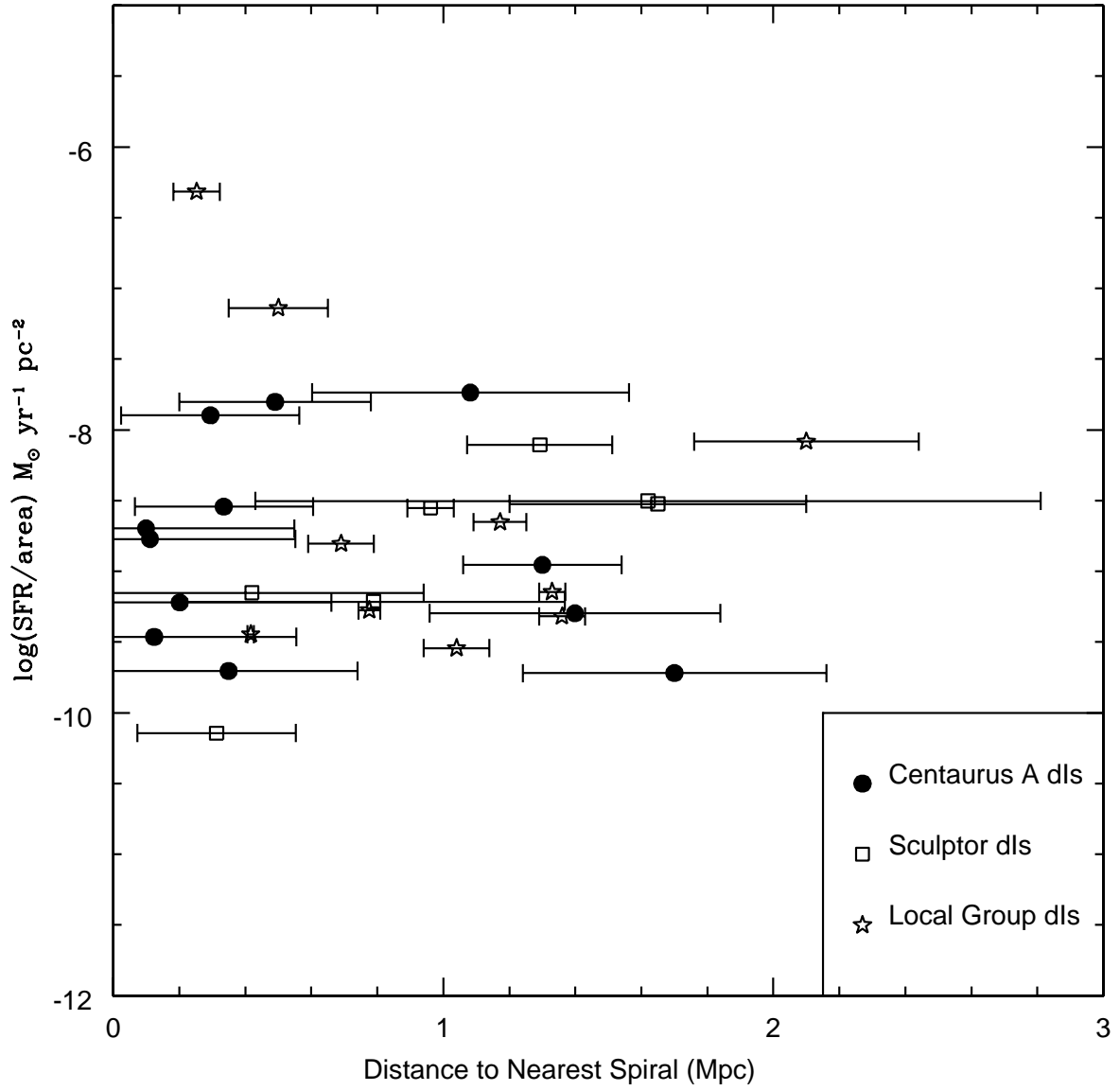


Fig. 8.— The star formation rates per unit area versus the distance to the nearest large galaxy in the group. As above, dots are for Centaurus A Group dIs, squares for Sculptor Group dIs and stars for Local Group dIs.

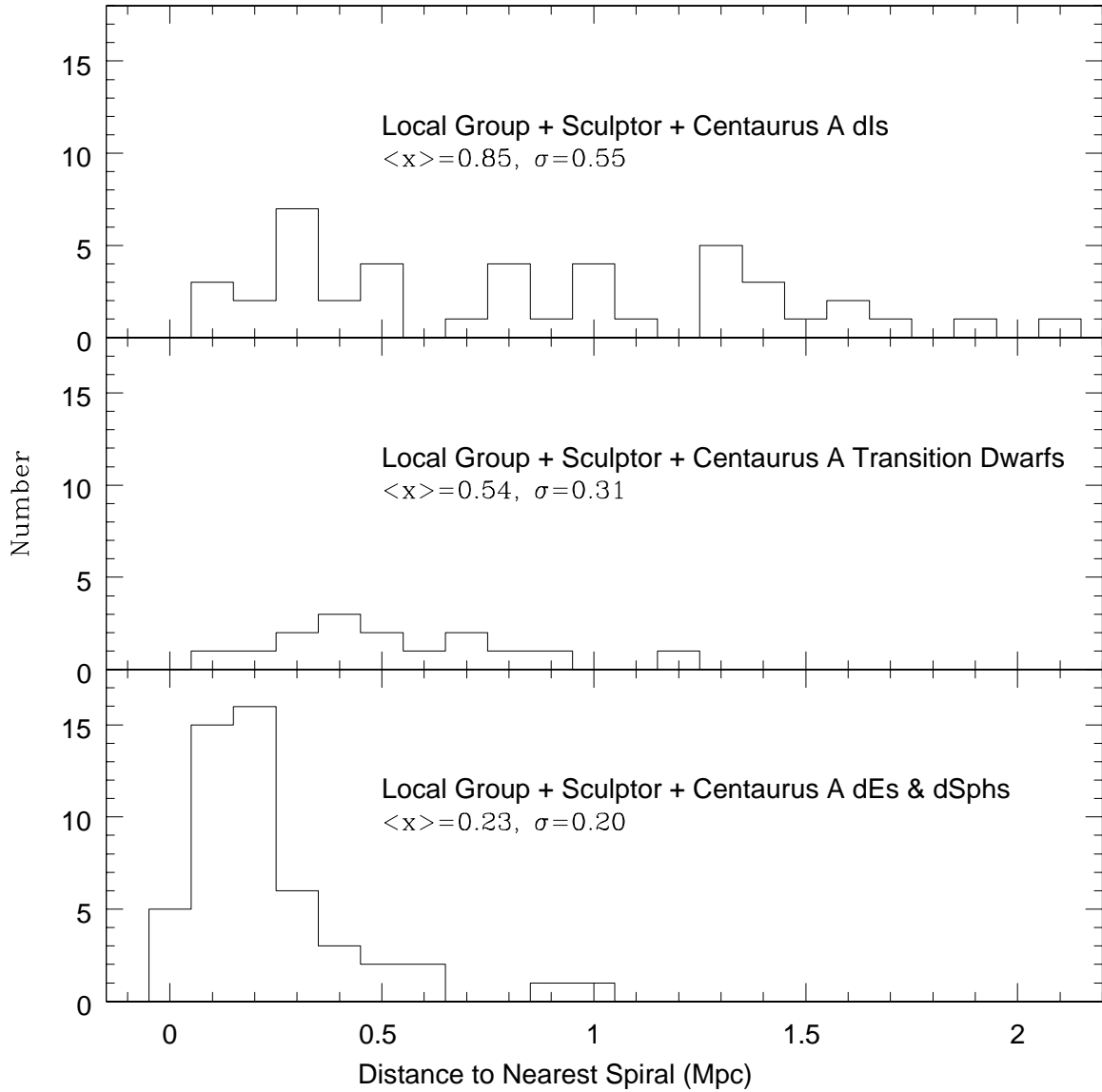


Fig. 9.— Histogram comparison of the distances to the nearest large galaxy of the group for the dI, transition, and dE galaxies in the Local Group, Sculptor Group and Centaurus A Group. For each sample the mean value and the standard deviation in the sample is given. On average the dIs lie at preferentially larger distances from the main galaxies of the group than the transition dwarfs, which are themselves at larger distances than the dEs.

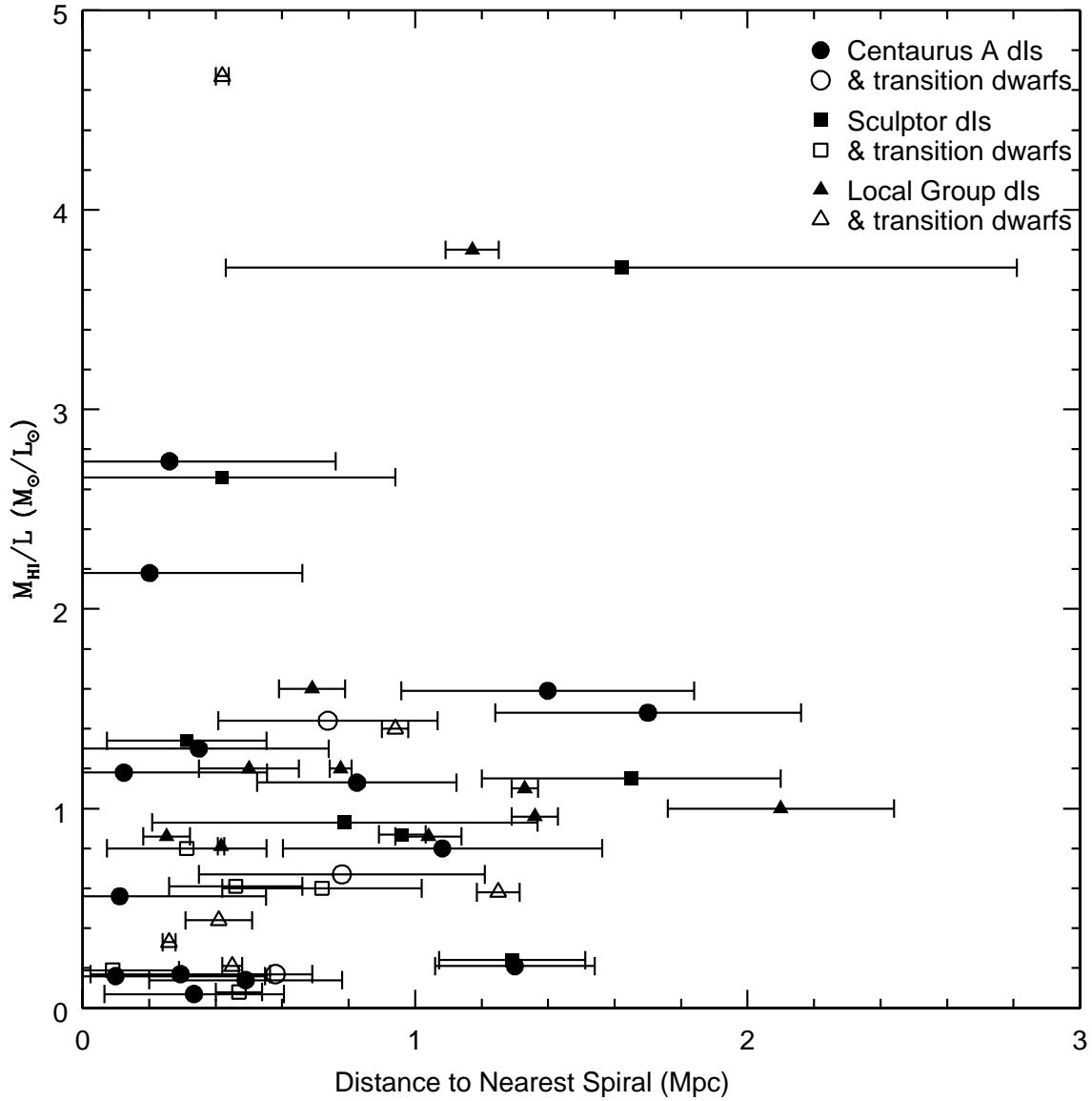


Fig. 10.— HI mass to light ratio M_{HI}/L is plotted versus the distance to the nearest large galaxy in the group. Full dots are for Centaurus A Group dIs, full squares for Sculptor Group dIs and full triangles for Local group dIs, while open symbols are for the transition dwarfs for each group respectively. The dIs closest to their primary galaxy are not less HI-rich than the dIs further out.

This figure "f1a.jpg" is available in "jpg" format from:

<http://arxiv.org/ps/0911.3879v1>

This figure "f1b.jpg" is available in "jpg" format from:

<http://arxiv.org/ps/0911.3879v1>

This figure "f1c.jpg" is available in "jpg" format from:

<http://arxiv.org/ps/0911.3879v1>

This figure "f1d.jpg" is available in "jpg" format from:

<http://arxiv.org/ps/0911.3879v1>

This figure "f1e.jpg" is available in "jpg" format from:

<http://arxiv.org/ps/0911.3879v1>

This figure "f1f.jpg" is available in "jpg" format from:

<http://arxiv.org/ps/0911.3879v1>